

The effect of doxorubicin encapsulated chitosan alginate nanoparticles and curcumin on multidrug resistant colon cancer cell lines



**UNIVERSITY of the
WESTERN CAPE**

Mutshidzi Audrey Masindi (4158378)

A mini thesis submitted in partial fulfilment of the requirements for the degree Magister Scientiae in the Department of Medical Bioscience, University of the Western Cape

Supervisor: Professor Star Khoza

Co-supervisor: Professor Admire Dube

TABLE OF CONTENTS

KEYWORDS	iv
ABSTRACT.....	v
DECLARATION	vii
ACKNOWLEDGEMENTS	viii
LIST OF ABBREVIATIONS	ix
LIST OF FIGURES.....	xi
CHAPTER 1: INTRODUCTION.....	1
CHAPTER 2: LITERATURE REVIEW	4
A. OVERVIEW OF MULTIDRUG RESISTANCE IN CANCER	4
2.1. Epidemiology of colorectal cancer.....	4
2.2. Colorectal cancer	4
2.3. Pathogenesis of colorectal cancer	5
2.4. Aetiology of colorectal cancer.....	7
2.5. Conventional methods used in treatment of colorectal cancer	7
2.7. P-glycoprotein inhibitors	12
B. NANOPARTICLES IN CANCER DRUG DISCOVERY	14
2.8. The use of nanoparticles to overcome multidrug resistance	14
2.9. Polymers used in the preparation of nanoparticles	14
2.10. Methods for the synthesis of CANPs	16
2.11. Previous attempts by to improve the delivery of DOX to increase the sensitivity of cancer cell.....	18
2.12. Physicochemical investigation of NPs	19
2.12.1. Dynamic light scattering analysis	19
2.12.2. Transmission electron microscopy.....	20
2.12.3. Scanning electron microscopy.....	20
CHAPTER 3: STUDY RATIONALE, HYPOTHESIS, AIMS AND OBJECTIVES.....	22
CHAPTER 4: SYNTHESIS AND CHARACTERIZATION OF DOXORUBICIN ENCAPSULATED ALGINATE CHITOSAN NANOPARTICLES	24
4.1. Introduction.....	24
4.1.1. Aim and objectives.....	24
4.2. Materials and reagents.....	24
4.3. Preparation of blank CANPs	25
4.4 Preparation of doxorubicin-encapsulated chitosan alginate nanoparticles	26
4.5. Physicochemical characterization.....	27
4.6. Statistical analysis	29

4.7. RESULTS AND DISCUSSION	30
CHAPTER 5: <i>IN VITRO</i> CYTOTOXICITY STUDIES	44
5.1. Introduction.....	44
5.1.1. Aims and objective	44
5.2. Materials and reagent.....	44
5.3. Methods	46
5.4. STATISTICAL ANALYSIS	51
5.5. RESULTS AND DISCUSSION	52
CHAPTER 6: CONCLUSIONS	58
CHAPTER 7: REFERENCE	59

KEYWORDS

Doxorubicin

Cancer

Chitosan

Alginate

Nanoparticles

Multidrug resistance

Ionic gelation

Polyelectrolyte

Curcumin

P-glycoprotein

ABSTRACT

Purpose: Although chemotherapeutic drugs have improved the survival rate of patients diagnosed with colorectal cancer, resistance to chemotherapy frequently leads to therapeutic failure and poor patient outcomes. Multidrug resistance (MDR) is a serious threat to cancer treatment efficacy and may be linked to the overexpression of drug efflux pumps. P-glycoprotein (P-gp) is a drug efflux transporter that triggers doxorubicin (DOX) resistance. This has led to an interest in chitosan alginate nanoparticles (CANPs) as novel anticancer drug carriers and curcumin (CUR) as an inhibitor of P-gp. Chitosan (CS) and alginate (ALG) are among the most extensively used polymers for nanoparticle (NP) preparation as they possess excellent non-toxic and biodegradable characteristics. The aim of this study was to investigate the effect of DOX encapsulated CANPs and CUR on MDR colon cancer cell lines (Caco-2 cells).

Method: Blank and DOX encapsulated CANPs were synthesized using the ionotropic gelation method. Thereafter, physicochemical characterization for size, polydispersity index and zeta potential were performed using dynamic light scattering (DLS). The morphology of both the blank and DOX encapsulated was characterized using the scanning electron microscope (SEM) and the transmission electron microscope (TEM). The fourier transform infrared spectroscopy (FTIR) was used to identify the functional groups in CS, ALG, blank CANPs and DOX encapsulated CANPs. The cytotoxicity of both the blank CANP and DOX-CANP with and without CUR on Caco-2 cells was assessed using the MTT assay.

Results: The results showed that the mean hydrodynamic diameter of the blank CANPs ranged from 279.44 ± 5.79 nm to 535.70 ± 39.62 nm and the negative zeta potentials ranged from -19.29 ± 1.67 mV to -25.20 ± 3.54 mV. The PDI for the blank

CANP ranged from 0.330 ± 0.03 to 0.840 ± 0.09 . The average hydrodynamic diameter of the DOX-CANPs ranged from 298.6 ± 38.10 nm to 761.4 ± 57.91 nm. The average PDI of the DOX-CANPs ranged from 0.359 ± 0.10 to 0.900 ± 0.14 . The average zeta potential of the DOX-CANPs ranged from -21.77 ± 5.11 mV to -26.34 ± 1.20 mV. The measured average core diameter was 80-90 nm ($n=15$) for both blank and encapsulated CANPs using TEM. SEM results illustrated that the blank and DOX-encapsulated CANPs formed aggregates and had inconsistent spherical shapes. DOX encapsulation efficiency ranged between 11.63%-15.97%. The DOX-CANPs decreased the cell viability of Caco-2 colon cell lines more than the blank CANPs (p -value ≤ 0.001) and DOX (p -value ≤ 0.001). The DOX-CANPs + CUR decreased cell viability of the Caco-2 colon cell lines more than the DOX-CANPs (p -value ≤ 0.001). The IC_{50} values for DOX and DOX-CANPs were 0.00123 ± 0.0003 and 0.00061 ± 0.0016 , respectively.

Conclusion: DOX encapsulated CANPs decreased the cell viability of multidrug resistant colon cancer cell line (Caco-2). CUR increased the efficacy of the DOX-CANPs against Caco-2 cell line.

DECLARATION

I declare that "*The effect of doxorubicin encapsulated chitosan alginate nanoparticles and curcumin on multidrug resistant colon cancer cell lines*" is my own work, that it has not been submitted for any degree or examination in this and any other university, and that all the sources I have used or quoted have been indicated and acknowledged by complete references.

Signed: 

Full name: Mutshidzi Audrey Masindi

Date: December 2023

ACKNOWLEDGEMENTS

I thank every single person who in one way or another contributed to the completion of this dissertation. There are no proper words to convey my deep gratitude and respect.

- First, I give thanks to God because it is by His grace that I am where I am today.
- Ms Valencia Jamalie and Prof Lindsay for the opportunity to complete my masters degree and for your support.
- I would like to express my special appreciation to my supervisors Prof Star Khoza and Prof Admire Dube. Thank you for your guidance and support throughout the jounery.
- To the Infectious Disease Nanomedicine group and MSc nanoscience class of 2021-2022, for their assistance and encouragement.
- To my family who encouraged me and prayed for me throughout the time of my research.
- This thesis is heartily dedicated to my late parents and grandparents. You are missed dearly.

LIST OF ABBREVIATIONS

CRC	- Colorectal cancer
CUR	- Curcumin
MDR	- Multidrug resistance
ABC	- ATP-Binding Cassette
ALG	- Alginate
ATCC	- American Type Culture Collection
CANPs	- Chitosan-alginate nanoparticles
DOX-CANP	- Doxorubicin encapsulated chitosan alginate nanoparticle
CS	- Chitosan
PBS	- Phosphate-buffered saline
h	- Hour
IG	- Ionotropic gelation
DLS	- Dynamic light scattering
FTIR	- Fourier transform infrared spectroscopy
NPs	- Nanoparticles
RT	- Room temperature
SEM	- Scanning electron microscopy
TEM	- Transmission electron microscopy
DMSO	- Dimethyl sulfoxide
ANOVA	- Analysis of Variance
DMEM	- Dulbecco's Modified Eagle's medium
DOX	- Doxorubicin
KRAS	- Kirsten rat sarcoma virus

APC

- Adenomatous polyposis coli

BBB

- Blood-brain barrier

LIST OF FIGURES

Figure 2. 1: Illustration of the CRC development (A) Histologic changes of CRC, when the number of cells inside the polyp start to increase rapidly (B) Acquired genetic changes of CRC, which correspond to adenomas and sessile serrated polyps	6
Figure 2. 2: The mechanisms of drug resistance in the cancer cells	11
Figure 2. 3: (a) The turmeric plant, (b) The turmeric rhizome with a yellow-orange interior, (c) The powdered form of turmeric, (d) The chemical structure of curcumin. (e) Demethoxycurcumin and (f) Bis-demethoxycurcumin.....	13
Figure 2. 4: Chemical structures of chitin and chitosan.....	15
Figure 2. 5: Structure of ALG-constituting blocks (G) 1,4 α -Guluronic acid (M) 1,4 β -D-Mannuronic acid	16
Figure 2. 6: The formation mechanism for Ca^{2+} -ALG. ALG reacts with CaCl_2 to generate Ca^{2+} -ALG, which is a gelatinous material	17
Figure 2. 7: The interaction between ALG as a polyanion and chitosan as polycation..	18
Figure 4. 1: Schematic diagram of method used to prepare alginate-chitosan nanoparticles.	26
Figure 4. 2 :Gelation procedure diagram; (a) shrinkage of sodium alginate; (b) crosslinking with calcium ions.....	30
Figure 4. 3: Size comparisons of blank CANPs with varying ALG-CS-Ca mass ratios (n=3).....	32
Figure 4. 4: PDI comparisons of blank CANPs with varying ALG-CS-Ca mass ratios (n=3).....	33

Figure 4. 5: Zeta potential comparisons of blank CANPs with varying ALG-CS-Ca mass ratios (n=3).)	34
Figure 4. 6: Standard curve generated for DOX, absorbance versus concentration (range 0.008 -1mg/ml), DI water measured at 480 nm wavelength	38
Figure 4. 7: The transmission electron microscope (TEM) image and size distribution for blank CANPs.	40
Figure 4. 8: The transmission electron microscope (TEM) image and size distribution of DOX encapsulated CANPs.	41
Figure 4. 9: The scanning electron microscope (SEM) image of (a) blank CANPs and (b)DOX encapsulated CANPs.	42
Figure 4. 10: FTIR spectra of alginate(black), chitosan (red), empty CANPs (blue), DOX loaded CANPs (green) and pure DOX (purple) registered in KBr pellets.	43

LIST OF TABLES

Table 4. 1: Hydrodynamic diameter, polydispersity index (PDI) and zeta potential of ALG-Ca-CS NPs. Data are provided as mean \pm S.D. (n = 3).....	31
Table 4. 2: Characterization of the synthesized DOX encapsulated CANPs.....	39
Table 5. 1: General information on the selected colon cell line.....	45
Table 5. 2: Experimental design	48
Table 5. 3: Plate layout for the cytotoxicity experiment	48
Table 5. 4: Plate layout for the combination experiment	51
Table 5. 5: IC ₅₀ values of the standard drug (DOX) and DOX-encapsulated CANPs on the Caco-2 cell line	53
Table 5. 6: IC ₅₀ values of DOX-encapsulated CANPs and DOX-CANP + CUR on the Caco-2 cell line.....	56

CHAPTER 1: INTRODUCTION

Colorectal cancer (CRC) is the second most common type of cancer accounting for the death of over 935 000 people annually (1). Globally, it is one of the cancers whose incidence is increasing and accounts for 11% of all cancer diagnoses. There was over 1.9 million new cases recorded in 2020 (2). It is estimated that by 2030, the burden of CRC will increase by 60% to over 2.2 million new cases and 1.1 million deaths. The incidence rates of CRC are higher in developed countries compared to developing countries (3). Approximately 25% of people with colon cancer will have synchronous metastatic disease, which will mostly affect the liver. Survival rates vary in each stage of colorectal cancer, reported to be 93.2% in stage I, 72.2 - 84.7% in stage II, 52.3 - 83.4% in stage III and 8.1% in stage IV (1).

Treatment for CRC has significant financial consequences. Most treatment expenses, including those for surgery, hospitalization, chemotherapy, immunotherapy, and post-acute care, are associated with the disease's early and terminal stages. The development of novel chemotherapeutics has resulted in an increase in treatment costs (4).

Chemotherapeutic multidrug resistance (MDR) is an enormous challenge in treatment for cancer patients. This prevalent and adverse clinical problem frequently results in cancer recurrence and low survival rate(5). Several studies reveal that this phenomenon results from the ability of cancer cells to become simultaneously resistant to many structurally and functionally unrelated drugs used in anticancer therapy (6). The over-expression of ATP-Binding Cassette (ABC) transporters is the most common mechanism by which cancer cells develop MDR. Increased drug efflux mediated by ABC transporters results in decreased intracellular drug accumulation,

and therefore decreased bioavailability (7). The development of methods that improve chemotherapy sensitivity and limit the adverse side effects are crucial in obtaining desired therapeutic outcomes and improved quality of life for patients(8).

Doxorubicin (DOX) use is linked to dose-dependent cardiotoxicity and multiple drug resistance leading to poor patient survival and prognosis (9, 10). DOX encapsulation in NPs may improve DOX's chemical stability, decreased cellular resistance, and decreased toxicity. A sustained release and selective delivery could lower the risk of a toxic effect, while the incorporation of DOX in the NP could reduce its degradation (11). DOX's cardiotoxicity may be reduced by natural polymers that have antioxidant activity, like CS without compromising how well the drug fights cancer(12).

Chitosan (CS) is a cationic, linear nitrogenous polysaccharide composed of glucosamine and N - acetyl-glucosamine linked by (1 → 4) β -glycosidic bonds (13, 14). It is a hydrophilic polymer obtained from the deacetylation of aminoacetyl groups of chitin which is the main component of the shells of crustaceans, the cell walls of fungi, and the cuticle of insects(15). In addition to the main properties of polysaccharides such as biocompatibility and biodegradability, the bio-adhesiveness of CS which facilitates the ionic interaction of positively charged amino groups of chitosan with negatively charged mucous layer is accountable for its usage as a promising material in the pharmaceutical industry (16).Alginate (ALG) is a hydrophilic anionic copolymer that is composed of alternating blocks of (1-4) linked β -D-mannuronic acid (M units) and -L-guluronic acid (G units) obtained from natural sources such as cell walls and intercellular spaces of marine brown algae and bacteria (17). The wide pharmaceutical applicability of ALG depends on its ability to form hydrogels by chelating with divalent cations (15).

Curcumin (CUR) is a bioactive component of turmeric, which was used in traditional Chinese medicine from ancient times (18, 19). It is reportedly making anti-cancer drugs more sensitive in MDR cancers and targets a variety of cancers. Despite the compound's promising pre-clinical activity, its limited water solubility and rapid metabolism prevent it from being used extensively in clinical settings (20).

Given this background, this study was conducted to determine whether DOX encapsulated chitosan alginate nanoparticles (CANPs) and CUR can increase the sensitivity of multidrug resistant colon cancer, using an *in vitro* cell line model. The study also characterized both the blank and DOX encapsulated CANPs.

CHAPTER 2: LITERATURE REVIEW

A. OVERVIEW OF MULTIDRUG RESISTANCE IN CANCER

2.1. Epidemiology of colorectal cancer

According to the World Health Organization, the global cancer burden was 19.3 million new cases and 10 million deaths in 2020 (21). This burden stems from several factors including an increase in population, aging, and an increase in cancers linked to social and economic development. This trend has also been noted in developing countries undergoing westernization. In particular, there is a significant increase in the prevalence of cancer cases associated with unhealthy diets and other detrimental lifestyle changes (22).

In South Africa, the CRC incidence rates have progressively increased over the years, with the annual crude incidence in male and female patients in 2014 reported as 7.34 and 5.86 per 100 000, respectively (23). CRC is most common within the white (Caucasian) population group in SA patients (52–54%), followed by black (African) (26–28%), coloured (mixed ancestry) (14–15%), and Asian (Indian) patients (4–7%) (23).

2.2. Colorectal cancer

Colon cancer is also known as colorectal cancer (CRC). CRC occurs in the colon and rectum and develops when the normal replacement of lining cells goes awry (24). The abnormal cells in the colon and rectum divide and grow rapidly, which results in the development of colon growths known as polyps. These polyps are precancerous tumours and are known to grow slowly and do not generally spread to distant parts of the body. As soon as there are any genetic mutations the cells become cancerous.

2.3. Pathogenesis of colorectal cancer

The progression of a non-cancerous polyp to colon carcinogenesis is not a once-off event but it is often a multistep process that leads to the accumulation of damage occurring during a lifetime. This process is complex and diverse, and it involves a series of histological, morphological and genetic alterations (25, 26).

2.3.1. Histological and morphological changes

Histological changes take place when the number of cells inside the polyp starts to increase rapidly, this then leads to an increase in the size of the polyp as illustrated in Figure 2.1 (A). These histological changes will lead to the accumulation of genetic mutations and epigenetic changes which are reflected by cytological and histologic dysplasia. As damage to the (deoxyribose nucleic acid) DNA increases over time, the features of high-grade dysplasia may develop. If the polyps are not removed at this stage, the polyps can break away leading to the development of secondary malignant growths away from the primary site of cancer (27).

2.3.2. Genetic changes

People can either acquire or inherit gene mutations. Inherited mutations, such as DNA mismatch repair genes and adenomatous polyposis coli (APC) gene mutations, are uncommon, most especially those associated with CRC. Approximately 5% of the population account for these cancers. The development of this CRC is a result of two main genetic pathways which correspond to adenomas and sessile serrated polyps as illustrated in Figure 2.1 (B). Adenomas are characterized by a series of mutations accumulating and are often associated with the instability of chromosomes. Typically, the mutations develop within the APC gene and Kirsten rat sarcoma virus (KRAS) oncogene, which affects chromatid migration to opposite poles of the nucleus and

downstream effects on cell growth, differentiation, motility, and survival. Over time, these mutations can cause a loss of function of the tumour protein P53 (P53) gene, which controls cell division and death. The development of the sessile serrated polyps tends to lead to mutations within the v-raf murine sarcoma viral oncogene homolog B1 (BRAF), which results in altered growth signalling and loss of apoptosis. KRAS mutations occur less frequently in sessile serrated polyps than in adenomatous polyps (27) and are known to be more prevalent in women (28).

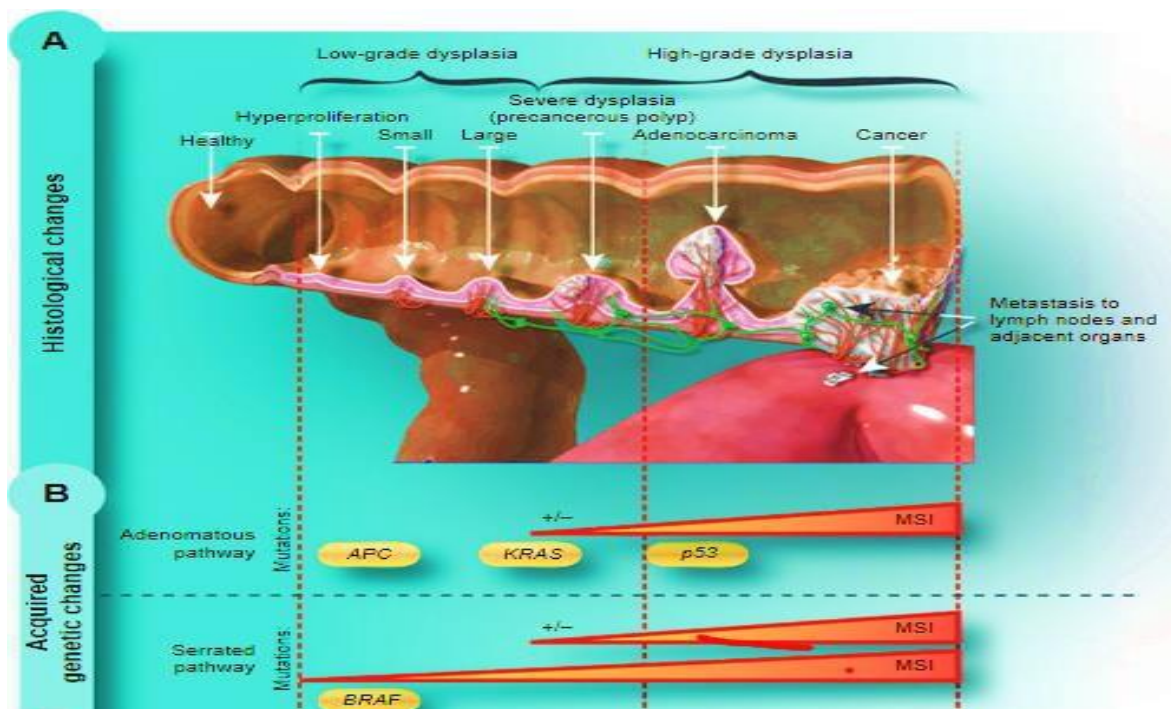


Figure 2. 1: Illustration of the CRC development (A) Histologic changes of CRC, when the number of cells inside the polyp start to increase rapidly (B) Acquired genetic changes of CRC, which correspond to adenomas and sessile serrated polyps

Key: (1) CRC-Colorectal cancer,(2) MSI- Microsatellite instability,(3) P53- tumour protein P53, (4) APC- Adenomatous polyposis coli,(5) KRAS- Kirsten rat sarcoma virus and (6) BRAF- v-raf murine sarcoma viral oncogene homolog B1 (26).

2.4. Aetiology of colorectal cancer

CRC is a disease that arises from multiple aetiologies such as genetics and lifestyle changes(29). Lifestyle-related cancers are more prevalent in economically transitional countries because they have developed unhealthy diets (high saturated fats, low fibre and fruits) and detrimental lifestyle changes such as physical inactivity, tobacco smoking and alcohol consumption (30). However, it has been estimated that 1-2% of CRC cases are associated with inflammatory conditions such as inflammatory bowel diseases (30).

2.5. Conventional methods used in treatment of colorectal cancer

2.5.1. Surgery

Surgery is the main treatment, and it is mostly affected by the stage of the tumour and localization. It adheres to the principle of removing the primary tumour and regional lymphatics with clear surgical margins (31). For CRC that has not spread, the best chance to cure will be through complete surgical resection (32).

2.5.2 Radiotherapy

Radiotherapy is used in different stages of CRC treatment to shrink the tumour before surgery and to kill cancer cells that may not be removed during surgery. It is also used as a palliative for advanced cancers, to decrease tumour size leading to down-staging advanced tumours and subsequently to prevent local recurrence (33). Sometimes a patient cannot undergo an operation, or the tumour is unresectable, and radiotherapy with/without chemotherapy can be considered as definitive treatment. It is also used in rectal cancer, because of the higher chance of relapse even after completing

surgical resection; postoperative radiotherapy is usually given aiming to reduce local and regional recurrence (32).

2.5.3 Chemotherapy

One of the current challenges in the treatment of cancer is severe side effects from treatment regimens leading to a lower the quality of life for cancer patients. Toxicity from current cancer treatments is associated with severe systemic side effects and drug resistance, resulting in increased morbidity and decreased survival among cancer patients (34). Although chemotherapy is used to induce cell death in cancerous cells, other normal cells which are rapidly dividing such as hair cells, also get affected. Generally, chemotherapy is given before (neoadjuvant) and/or after (adjuvant) surgery. Adjuvant chemotherapy is offered to people with advanced CRC as an additional treatment to destroy cancerous cells that remain in the body to prevent the recurrence of cancer. Neoadjuvant chemotherapy is usually administered before surgery is performed to shrink the tumour (35-37).

2.5.3.1. Doxorubicin

Doxorubicin is one of the first identified anthracyclines and is known as adriamycin (38). It inhibits the proliferation of cancerous cells in the body by blocking the deoxyribose nucleic acid (DNA) topoisomerase II catalytic enzyme which is essential for the survival of the cells in the body, and it also intercalates the DNA (39).

DOX is a parent drug of its major metabolite, doxorubicinol (40). Around 74-76% of doxorubicinol is bound to plasma proteins and rapidly taken up by the tissues in the human body (41). It does not reach the brain because it cannot cross the blood-brain

barrier (BBB) and it has a half-life of 20-48 hours. There are three metabolic pathways of DOX namely: one-electron reduction, two-electron reduction, and deglycosidation. The one-electron reduction pathway yields a doxorubicin-semiquinone radical; the two-electron pathway yields doxorubicinol; while the deglycosidation pathway yields one of two metabolites, deoxyaglycone or hydroxyaglycone. The metabolites produced can either augment or inhibit the anticancer properties of DOX. The route of elimination is through urine (42).

2.5.3.2. Limitations of doxorubicin

(i) Cardiotoxicity

Doxorubicin has several mechanisms of action. The pathways which are mostly involved in the related cardiac toxicity is currently unknown. Numerous studies suggest that heart failure may be brought on by the production of reactive oxygen species during doxorubicin treatment and the resulting lipid peroxidation, calcium dysregulation, and interference with energy transmission. The underlying molecular causes of its toxicity have not been fully understood (43).

(ii) Drug resistance

Failure in chemotherapy is common because of drug resistance. Drug resistance is one of the major factors that lead to the poor response to anticancer agents. It is often characterized by decreased sensitivity of cells to cancer treatments and resistance to apoptosis. Anticancer drug resistance can be intrinsic (inherited) or acquired during treatment by tumours that are initially sensitive to chemotherapy, which is also known as target specific mechanism (44).

2.6. Multidrug resistance

Patients can develop resistance to drugs that are structurally and functionally unrelated, a phenomenon referred to as multidrug resistance (MDR) (45). Patients who develop resistance to the first chemotherapeutic drug are more likely to develop resistance to a second chemotherapeutic drug. MDR mechanisms are classified into non-cellular MDR and cellular MDR. The non-cellular MDR is mainly due to extracellular factors and cellular MDR involves intracellular factors such as drug targets and enzymes inside the cell. Cellular MDR is classified into transport-based MDR phenotypes and non-transport-based MDR phenotypes. An example of the non-transport based includes evasion of apoptosis and the transport-based phenotype is the ATP-Binding Cassette (ABC) transporters which are proteins responsible for the intracellular increase in drug efflux (46).

2.6.1. Main mechanisms that can converge in drug resistance

Drug resistance is caused by several factors which include the following: (1) increase in drug efflux from the cell by adenosine triphosphate (ATP)-dependent transporters such as P-glycoprotein, breast cancer resistance protein and the multidrug resistance-associated protein, (2) drug inactivation, (3) alterations in the drug target, (4) DNA damage repair, (5) cell death inhibition, (6) epithelial-mesenchymal transitions (EMT) and (7) epigenetic effects as shown in Figure 2.2. The stromal cells aid in the EMT process and signal the cancer cells to become more resistant. Factors that control EMT are also secreted by cancer cells and stromal cells (47).

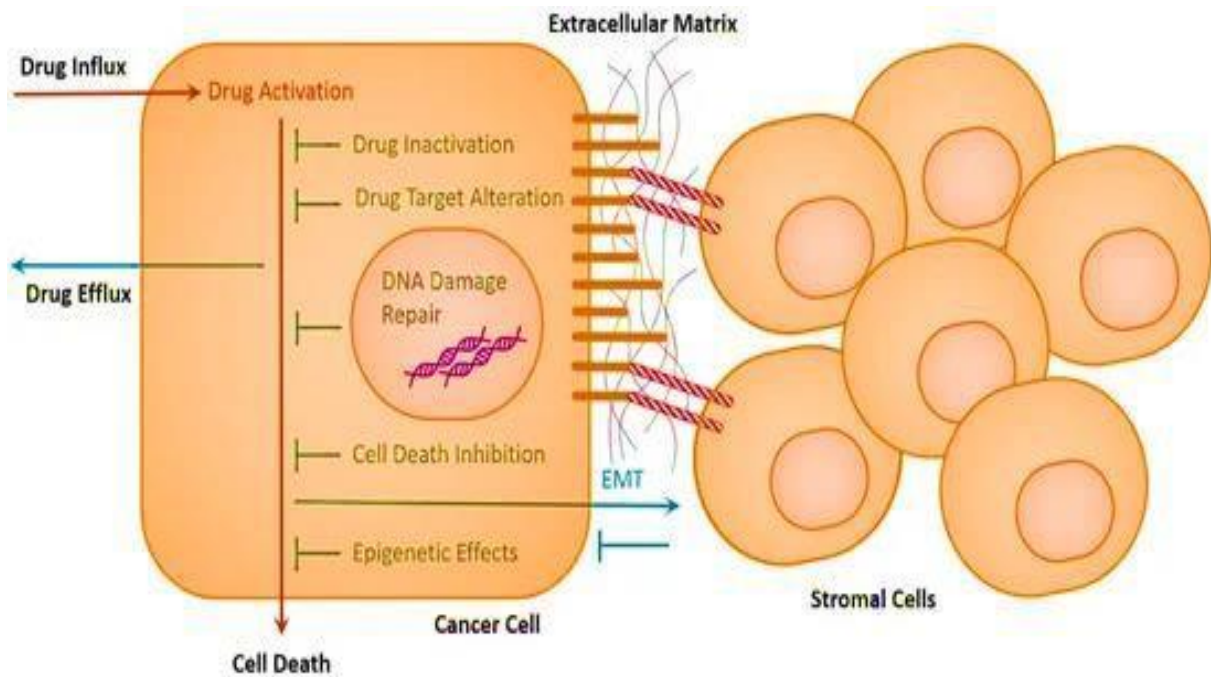


Figure 2. 2: The mechanisms of drug resistance in the cancer cells. These include drug inactivation, alteration of drug targets, drug efflux, DNA damage repair, inhibition of cell death, EMT, and epigenetic effects. Stromal cells aid in the EMT process and signal to cancer cells to become more drug resistant. Cancer cells' cell adhesion molecules bind to extracellular matrix proteins and stromal cells' cell adhesion molecules. Factors that control EMT are also secreted by cancer cells and stromal cells. An abridged illustration of these cell interactions is shown (47).

Resistance may occur due to the presence of more than one factor after exposure to a chemotherapeutic agent on cancer cells, a phenomenon known as multifactorial drug resistance (48).

2.6.1.1. ATP-binding cassette transporters

The ABC superfamily has different types of transporters: P-glycoprotein (P-gp/ABCB1), multidrug-resistant protein 1 (ABCC1), and breast cancer-resistant protein (BCRP/ ABCG2) transporters (49).

(i) P-glycoprotein

P-glycoprotein is a transmembrane protein that belongs to a family of transporters and is encoded by the ABCB1 gene. P-glycoprotein has a molecular weight of 170 kDa. This protein is known for transporting only large, lipophilic, and positively charged compounds (49). P-glycoproteins are the primary determinant of multidrug resistance (50).

(ii) Multidrug resistance-associated protein

MDR-associated protein is a membrane transporter that also causes the resistance of some chemotherapeutic drugs because of the increase in drug efflux out of the cells. The protein is encoded by the ABCC1 gene and has a molecular weight of 190-kDa (51). This protein preferentially transports unconjugated and conjugated organic anions (49).

2.7. P-glycoprotein inhibitors

2.7.1. Curcumin

Curcumin (CUR) is a secondary metabolite isolated from the turmeric of *Curcuma longa* and has been traditionally used for many years in Southern Asia (52). This yellowish colour is because of the presence of curcuminoids as shown in Figure 2.3 a-c, which are natural polyphenol compounds classified into three diarylheptanoids:

CUR (77%), demethoxycurcumin (17%), bisdemethoxycurcumin (3–6%) as shown in Figure 2.3 d-f and other less abundant secondary metabolites (53).

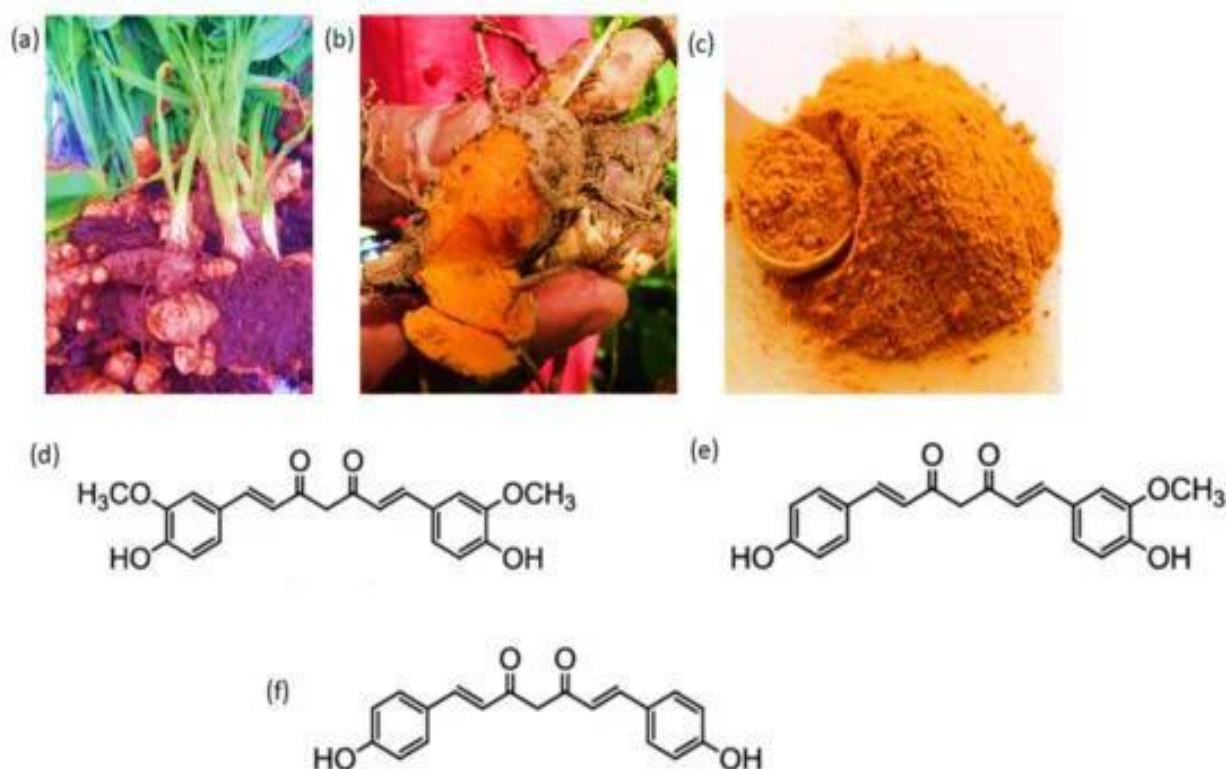


Figure 2. 3: (a) The turmeric plant, (b) The turmeric rhizome with a yellow-orange interior, (c) The powdered form of turmeric, (d) The chemical structure of CUR. (e) Demethoxycurcumin and (f) Bis-demethoxycurcumin (53).

CUR is one of the most well-known natural modulators, and it has been observed to restore drug sensitivity in cancer cells by overexpressing the MDR-related ABC transporters P-gp, MRP1, and ABCG2 in combination with other anti-cancer drugs. CUR interacts directly with the drug binding site of the transporter, although it is not a substrate for P-gp. It is able to significantly lower the P-gp expression and reduce the function of P-gp (54). A study by (55) reported that CUR stimulates the ATPase activity of MRP1 at low concentration, but inhibition of activity at higher concentration, which can be attributed to CUR's interaction with MRP1's binding site. It is not the protein levels of ABCG2 that cause the reversal of resistance, but their

impact on its function(56). However, poor bioavailability, rapid metabolism due to its lipophilic, and highly insoluble nature, and being effective in high doses, are among the major problems encountered when using CUR clinically (57-59).

B. NANOPARTICLES IN DRUG DELIVERY

2.8. The use of nanoparticles to overcome multidrug resistance

NP based drug delivery platforms have been extensively studied for cancer diagnosis and treatment and have emerged as optimal carriers for overcoming limitations encountered with conventional drug formulations by influencing ABC transporter-associated drug efflux mechanisms. Polymeric and solid lipid NPs, liposomes, micelles, mesoporous silica NPs, dendrimers, and nanostructured lipid carriers are the major classes of nanocarriers used to overcome MDR (60-62).

2.9. Polymers used in the preparation of nanoparticles

The properties of polymeric NPs are highly dependent on the type of polymer used in their preparation (63). These polymers can be divided into two groups, that is synthetic polymers e.g., polylactic acid and polylactic-co-glycolic acid NPs, and naturally occurring polymers e.g., CS and ALG (64). CS and ALG are among the most extensively used polymers for NP preparation because they possess excellent non-toxic and biodegradable characteristics (65).

2.9.1 Chitosan

CS is a cationic polymer derived from chitin; found in the exoskeletons of crustaceans (66). It is obtained through deproteination and demineralization (through sequential treatment with sodium hydroxide and acid) and deacetylation (the removal of acetyl groups on the polymer chain) of chitin (67). CS is composed of linear β (1 \rightarrow 4)-linked 2-amino-2-deoxy- β -D-glucose and 2-acetomido-2-deoxy β -D-glucose residues as shown in Figure 2.4 (68). It has an essential polycationic property, as evidenced by its pKa value of 6.5; in acidic solutions, the amino groups (NH₂) on the backbone of chitosan become protonated and positively charged (NH₃⁺), rendering CS soluble in

aqueous acidic solutions; in an alkaline environment, the amino groups lose their positive charges, rendering CS insoluble (69).

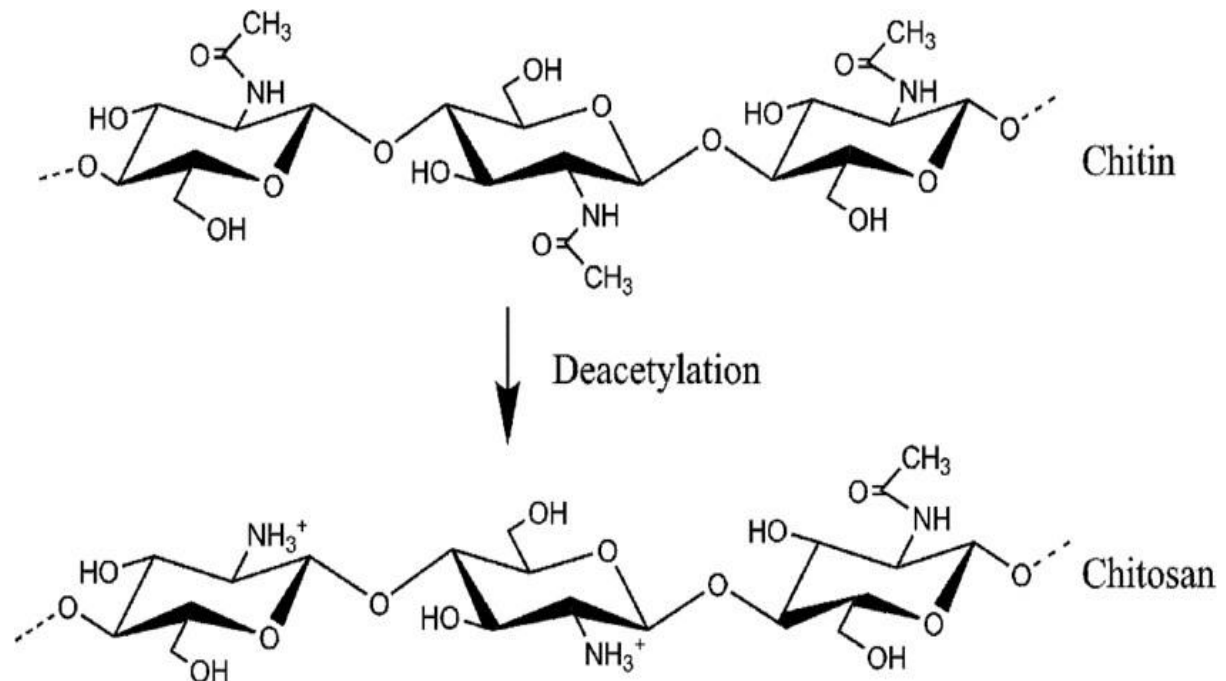


Figure 2. 4: Chemical structures of chitin and chitosan. Chitosan is obtained by deacetylation of chitin, where acetate ions ($C_2H_3O_2^-$) and the amino group ($-NH_2$) are produced through hydrolysis of acetamide group (CH_3CONH_2) (68).

2.9.2 Alginate

ALG, like CS, is also a biopolymer and is derived from brown algae. Chemically, ALG is composed of 1-4 linked α -L-guluronic (G) and β -D-mannuronic acid residues (M) (70). The ratio and sequential order of the G and M residues vary in different ALG species and are known to affect the physicochemical properties of ALG which have biological importance (71).

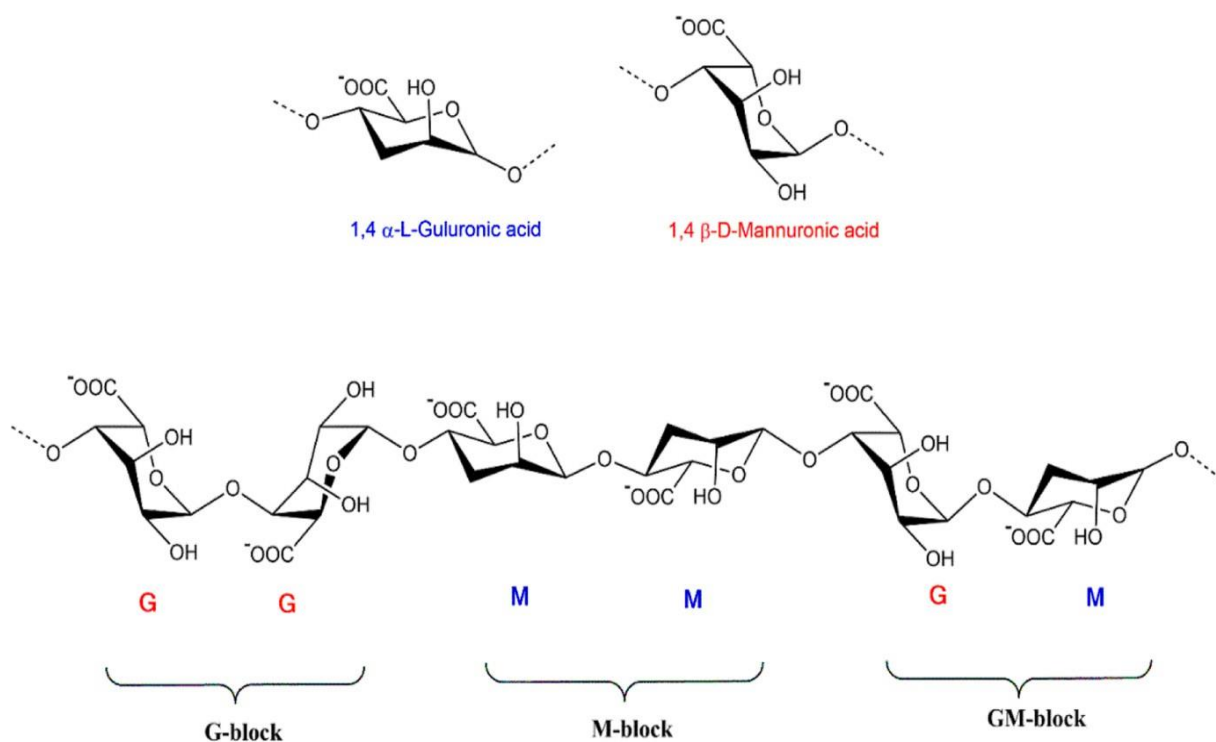


Figure 2. 5: Structure of ALG-constituting blocks (G) 1,4 α -Guluronic acid (M) 1,4 β -D-Mannuronic acid (70).

2.10. Methods for the synthesis of CANPs

Several methods can be carried out for the synthesis of NPs based on a combination of CS and ALG (72).

2.10.1. Ionotropic pre-gelation

Alginate (ALG) reacts with calcium chloride (CaCl_2) to generate Ca^{2+} -ALG, which is a gelatinous material. The two chemicals are rearranged, so they bond (like the eggbox model) to form a gelatinous substance as shown in Figure 2.6 (73). An important property of the application of ALG for nanoencapsulation of drugs is the fact that the polymer solution forms a reversible gel when ionically crosslinked with multivalent cations such as Ca^{2+} , enabling drug retention within the gel matrix (74, 75). The sequence of guluronic acid residues arranged in side-by-side blocks is believed to be responsible for the gelling

property due to high selectivity. Thus, the properties of ALG gel change with the composition of G- and M-residues, with their sequential order, and with the molecular weight of the polymer and concentration of counterions during gelation (75).

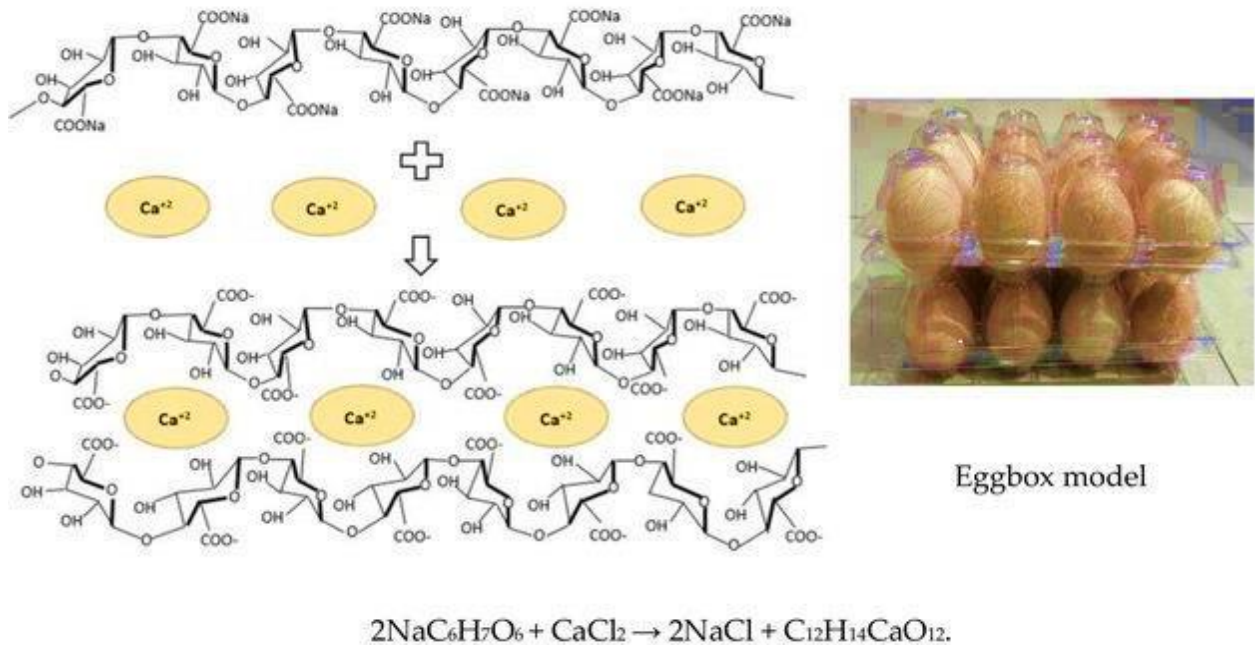


Figure 2. 6: The formation mechanism for Ca^{2+} -ALG. ALG reacts with CaCl_2 to generate Ca^{2+} -ALG, which is a gelatinous material. The two chemicals are rearranged, so they bond (like the eggbox model) to form a gelatinous (jello-like) substance (73).

2.10.2. Polyelectrolyte complexation

The polyelectrolyte network is formed by the interaction between the dissociated functional groups: an anionic carboxyl group of ALGs and a cationic amino group of CS, intra- and inter-chain hydrogen bonding between different parts of the polysaccharides' structures and between already created aggregates of CANPs (76). The complexation of polyelectrolytes leads to coacervate and hydrogel formation or precipitation. The occurrence of these processes depends on the reagent concentration, ionic strength, pH, temperature, order of mixing, the flexibility of

polymers, and the chemical composition of polymers (77). Polyelectrolyte complexes from CS and ALG may be formed by various methods; a one-step process involves the gradual addition of CS solution to ALG. The subsequent addition of an aqueous polycationic solution (CS) result in a polyelectrolyte complex, stabilizing the ALG pre-gel nucleus into individual sponge-like NPs. This pre-gelation methodology was first described by Rajaonarivony *et al.* and applied to the encapsulation of DOX (78).

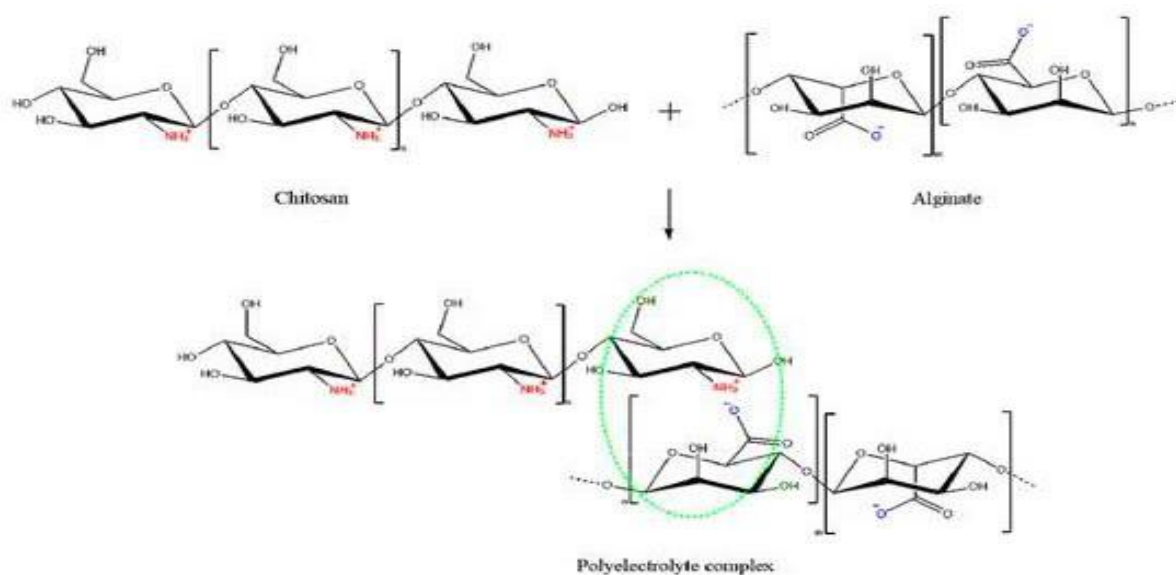


Figure 2. 7: The interaction between ALG as a polyanion and chitosan as polycation. The oppositely charged polyelectrolytes lead to formation of a polyelectrolyte complex caused by the electrostatic interactions between the NH⁺ ions from chitosan and O⁻ ions from ALG (69).

2.11. Previous attempts to improve the delivery of DOX to increase the sensitivity of cancer cell

A study by (79) evaluated DOX encapsulated in CANPs to reduce both the viability of melanoma cells and the tumour growth in a mouse melanoma model. The free and encapsulated DOX decreased the viability of melanoma cell lines to a similar degree. However, the cytotoxic effect of the encapsulated DOX still occurred in the more

resistant cells even after removing the extracellular drug. The experiments on a syngeneic melanoma mouse model revealed that free and encapsulated DOX elicited the control of the tumour growth. Thus, the encapsulation of DOX into CANPs could be considered advantageous because of the better intracellular accumulation and longer cytotoxic effect on the investigated melanoma cells (79). (15) evaluated the cytotoxicity of DOX released from the CANPs and showed a notable difference in comparison with that of free DOX on the MCF-7 cell line.(80) evaluated the impact of DOX encapsulation in CANPs on its stability, cytotoxic potential in multidrug-resistant lymphoma cells (L5178 MDR1), and toxicity in H9c2 cardioblasts. The results indicated that the encapsulation stabilized the drug against degradation due to its inner location in nanoparticles as suggested by thermogravimetric and X-ray diffraction analyses. Further, the encapsulated DOX was significantly more cytotoxic to L5178 MDR1 cells than free DOX.

2.12. Physicochemical investigation of NPs

2.12.1. Dynamic light scattering analysis.

Dynamic light scattering (DLS) analysis, also known as quasi-elastic light scattering, is a technique used to characterize NPs using the Brownian motion (diffusion) and subsequent size distribution of an ensemble collection of particles in solution. The measured scattering intensity will fluctuate with time for particles moving under the influence of Brownian motion. Correlation is a statistical method for measuring the degree of non-randomness in a random data set. The advantages of the method are the speed of analysis, lack of required calibration, and sensitivity to submicrometer particles (81, 82).

2.12.2. Transmission electron microscopy

Transmission electron microscopy (TEM) has a smaller size limit of detection, is a good validation for other methods, and affords structural requirements, and one must be cognizant of the statistically small sample size and the effect that vacuum can have on the particles (83). TEM utilizes electrons instead of light as a “light source” and their much lower wavelength makes it possible to get a visual resolution a thousand times better than with a light microscope (84).

2.12.3. Scanning electron microscopy

Scanning electron microscopy (SEM) is a surface imaging method in which the incident electron beam scans across the sample surface and interacts with the sample to generate signals reflecting the atomic composition and topographic detail of the specimen surface (85-87). The incident electrons cause emissions of elastic scattering of electrons, referring to backscattered electrons, inelastic scattering of electrons named low-energy secondary electrons, and characteristic X-ray light called cathodoluminescence from the atoms on the sample surface or near-surface material (88). The size, size distribution and shape of nanomaterials can be directly acquired from SEM (89).

2.12.4. Fourier transform infrared (FTIR) spectroscopic technique

FTIR offers analysis for organic and inorganic samples (90). It identifies chemical bonds in a molecule by producing an infrared absorption spectrum (91). The spectra create a sample profile, or characteristic molecular fingerprint, that can be used to check samples for a variety of different elements (92).

2.13. Cytotoxicity of NPs

The cytotoxicity study is an important step in testing NPs in the context of biological and medical applications. Assays based on tetrazolium salts, like MTT (2-(4,5-dimethyl-2-thiazolyl)-3,5-diphenyl-2H-tetrazolium bromide), nitroblue tetrazolium (NBT) and the second-generation tetrazolium salts, such as XTT (sodium 2,3-bis(2-methoxy-4-nitro-5-sulfophenyl)-5-[(phenylamino)-carbonyl]-2H-tetrazolium inner salt), MTS (5-[3-(carboxymethoxy)phenyl]-3-(4,5-dimethyl-2-thiazolyl)-2-(4-sulfophenyl)-2H-tetrazolium inner salt) and WST-1 (sodium 5-(2,4-disulfophenyl)-2-(4-iodophenyl)-3-(4-nitrophenyl)-2H-tetrazolium inner salt) are basic tools for cytotoxicity determination (93).

2.13.1. The use of MTT to study MDR

Drug sensitivity can be assessed by the colorimetric MTT assay (94). The concept of sensitization involves making the drug resistant cancer cells sensitive to the same or different drugs, in order to develop a successful therapeutic regimen (95)(92).

2.14. Caco-2 as a model for studying MDR

The human Caco-2 cell line is a widely used in vitro model of the intestinal epithelial barrier (96). The Caco-2 cell line is the best-characterized model for the human small intestine because the cells differentiate into enterocyte-like cells that express brush border membrane enzymes(97, 98). The expression of several ABC transporters, P-gp and BCRP are expressed in caco-2 cell line(99).

CHAPTER 3: STUDY RATIONALE, HYPOTHESIS, AIMS AND OBJECTIVES

3.1. Study rationale

At present, a variety of treatment regimens and combinations of drugs are used in the treatment of CRC (100). Although chemotherapeutic agents have improved the survival rate of CRC patients, they have many limitations including poor absorption, non-specific distribution, drug resistance, severe side effects, and low response (101). Its effectiveness and utility as a therapeutic strategy would be significantly increased by reducing these negative effects. This has led the study to explore CANPs as a drug delivery system to improve treatment outcomes in patients with CRC. Drug delivery systems (DDS) show various advantages as compared to conventional chemotherapy

(102). They can deliver the drug to a specific tumour site, facilitate drug clearance from the circulatory and immune system, alter the physicochemical properties of drugs, reduce the dose needed and control the drug release; such characteristics give DDS great potential for cancer therapy (103, 104). DOX is one of the most effective drugs for the treatment of solid tumors and functions mainly through DNA insertion and topoisomerase II inhibition to achieve apoptosis and the inhibition of cell growth (105). However, the emergence of MDR (by the P-gp pathway), strong cell toxicity, and poor targeting selection have seriously hindered its clinical application (106). CUR is a low-toxicity natural drug and is less effective against cancer than first-line chemotherapy but has excellent effects (107-109). CUR has a protective effect on DOX toxicity in the heart, kidney, liver, and blood components. Therefore, the co-delivery of CUR and DOX could be an effective combination chemotherapy but further investigation is required (110). For this purpose, this study investigated the cytotoxicity of DOX-

encapsulated CANPs on Caco-2 cell line and in combination with CUR on the Caco-2 cell lines.

3.2. Hypothesis

The co-delivery of DOX encapsulated CANPs and CUR will decrease multidrug resistance in colon cancer cell lines

3.3. Aim of the study

To determine the potential of the co-delivery of DOX encapsulated CANPs and curcumin as sensitizing agents in multidrug-resistant (Caco-2(ATCC® HTB-37™)) colon cancer cells.

3.4. Objectives

- To prepare DOX encapsulated CANPs.
- To characterize the physicochemical properties of the blank and DOX encapsulated CANPs.
- To determine the cytotoxicity effects of DOX encapsulated CANPs and CUR, on the multidrug-resistant (Caco-2(ATCC® HTB-37™)) colon cancer cell lines using 3-(4, 5-dimethylthiazol-2-yl)-2, 5-diphenyltetrazolium bromide (MTT) assay.

CHAPTER 4: SYNTHESIS AND CHARACTERIZATION OF DOXORUBICIN ENCAPSULATED ALGINATE CHITOSAN NANOPARTICLES

4.1. Introduction

This chapter describes the synthesis and characterization of both the blank and DOX encapsulated CANPs. The characterization techniques include dynamic light scattering (DLS), transmission electron microscopy (TEM), scanning electron microscopy (SEM) and Fourier transform infrared spectroscopy (FTIR).

4.1.1. Aim and objectives.

The aim for this part of the study was to synthesize and characterize blank and DOX encapsulated CANPs. The primary objective was to synthesize CANPs using the same concentration of ALG and different concentrations of CS and CaCl₂, to select the best formulation and to characterize the physicochemical properties. The second objective was to encapsulate DOX and to characterize DOX encapsulated CANPs.

4.2. Materials and reagents

Apparatus

Analytical balance (Ohaus®, model GA 110), UV-Violet spectrophotometer (Cintra 202, GBC Scientific Equipment, Australia), XS Instruments Eutech instruments pH 2700 (Wirsam), WH200 hot plate/stirrer (Wiggens), Heraeus™ Biofuge13™ Centrifuge (Thermo Fisher Scientific (USA)), Malvern Zetasizer Nano ZS-90 (Malvern (UK)), Scientech™ Ultrasonic Cleaner (ScienTech (USA)), Probe sonicator (Sonoplus GM 2070, Bandelin, Germany), Transmission electron microscope (Thermo fisher (FEI), Eindhoven, Netherlands), Tescan MIRA SEM, PerkinElmer 400 FTIR spectrophotometer (Perkin Elmer, Waltham, USA). Ultralow -86 °C freezer (NU-9668E,

NuAire, USA), Centrifuge (Digicen 21, Orto Alresa, United Scientific), 0.45 μ m Nylon syringe filter (Membrane solutions), Pipette tips 20,100,200,1000 μ l (Lasec, South Africa), Needles (Merck, Germany), Micropipette 10,20,200,1000 μ l (DLAB, China).

Chemicals and reagents

DOX hydrochloride, Calcium chloride (anhydrous, powder, $\geq 97\%$) was purchased from Sigma-Aldrich (Japan), Glacial acetic acid, potassium bromide, Chitosan (low molecular weight) was purchased from Sigma-Aldrich (Iceland), Phosphate buffered saline (PBS) pH 7.4, Sodium Alginate was purchased from Sigma-Aldrich (United Kingdom), deionized water was obtained from a Barnstead Easy Pure(II) UV-ultrapure water system (Thermo Fisher Scientific, USA). Sodium hydroxide pellets (Merck, South Africa), Hydrochloric acid (B & M SCIENTIFIC, South Africa). All other chemicals were of analytical grade unless where otherwise stated.

4.3. Preparation of blank CANPs

The CANPs were prepared using a slightly modified method adapted from (111). Solutions of ALG (0.06% w/v) and CS (0.1% w/v in 1% acetic acid) were separately prepared in dH₂O and left stirring overnight at room temperature. Thereafter, the ALG and CS solutions were filtered through a 0.45 μ m filter, and their pH adjusted to 4.9 and 4.6, respectively. The pH of the ALG solution was adjusted to 4.9 using hydrochloric acid and the CS solution was adjusted to 5.6 using sodium hydroxide. These pH values (4.6 and 4.9) were chosen because CS and ALG interact more strongly at acidic pH levels, which results in the formation of more compact particles (112, 113). The CS solution was made up to varying concentrations (0.02%, 0.05%, 0.08% w/v in dH₂O) and the ALG solution was kept at a constant concentration (0.06%). A CaCl₂ solution was prepared in dH₂O at varying concentrations (0.04%,

0.067%, 0.1% w/v) and the pH adjusted to 4.8 using hydrochloric acid and sodium hydroxide. All materials were filtered through 0.45 μm membranes prior to use. The CaCl_2 solution (2 ml) was added drop wise to the ALG solution (10 ml) under probe sonication (50% power) for

3 minutes and allowed to stand on ice for 1 minutes; to form the pre-gel. Following this, the CS solution (1.5 ml) was added drop wise to the pre-gel solution under probe sonication (50% power) for 3 minutes. This resulted in a colloidal suspension. The NPs were recovered by centrifugation at 8000 x g for 30 min, washed and stored at 4°C in dH₂O (pH 5). Following this, the NPs were kept at -80°C and then freeze-dried for 48 hrs producing a fine, white powder for further analysis.

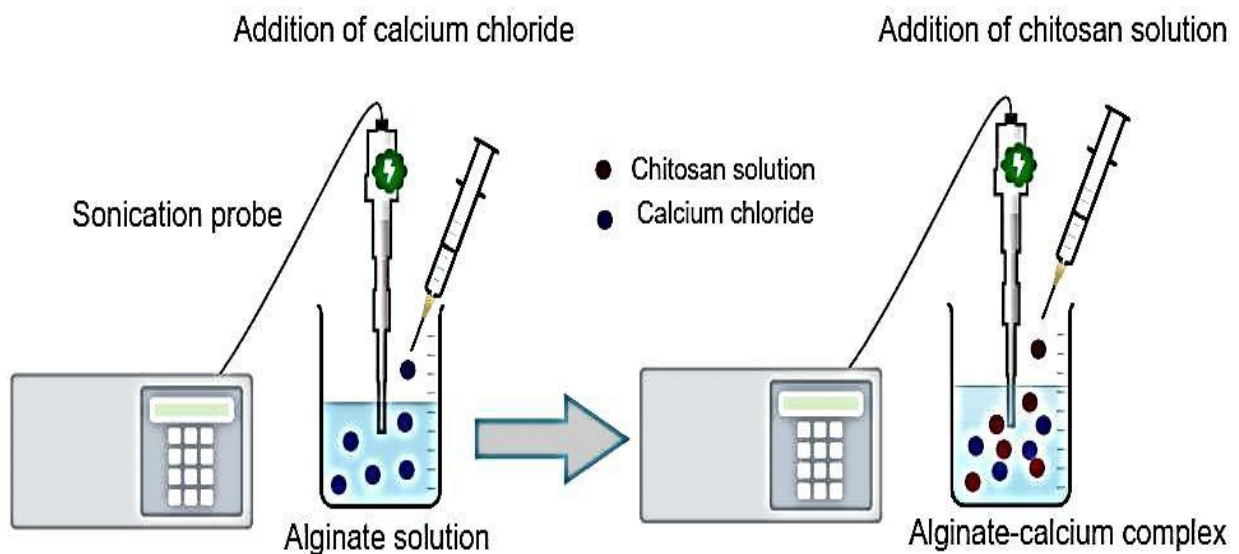


Figure 4. 1: Schematic diagram of method used to prepare CANPs. Calcium chloride solution was added to ALG solution, and CS solution was added to create polyelectrolyte complexes during sonication.

4.4 Preparation of doxorubicin-encapsulated chitosan alginate nanoparticles

The synthesis of CANPs described in section 4.2 was modified to encapsulate the doxorubicin into the CANPs. Varying concentrations of DOX (0.06, 0.04, 0.02, 0.01, 0.005, 0.0025, 0.00125, 0.000625 w/v) were added to the ALG solution and bath sonicated, at high frequency, for 2 min. The rest of the method was then followed as described in 4.2 to form DOX-CANPs. The DOX encapsulated CANPs were recovered by centrifugation at 18 000 x g for 30 min, washed twice with dH₂O at pH 5 and the

NPs were kept at -80°C overnight and then freeze-dried for 48hrs producing a fine, reddish powder.

4.5. Physicochemical characterization

4.5.1. Dynamic Light scattering analysis and Electrophoretic light scattering

The size, PDI and zeta potential of the synthesized chitosan-alginate nanoparticles were evaluated by the Malvern Zetasizer Nano ZS90 at the Department of Biotechnology, University of the Western Cape. The nanoparticles were washed and resuspended in deionized water (pH 5) and were measured. A sample of 1 ml was taken for z-average size and PDI determination after washing. It was then be transferred to a 12 mm disposable plastic cuvette and placed into the instrument. The intensity-weighted mean value was measured and the average of three measurements was taken. For zeta potential characterization, a disposable folded capillary cell was rinsed with distilled water using a 1 ml syringe prior to analyses as recommended by the manufacturer and 700 µl of nanoparticle solution will be added to the cell. The samples will then be analyzed with a voltage of 4 mV at 25°C at an angle of 173° to the laser beam. The intensity weighted mean value was measured and the average of three measurements were taken. The same was done on DOX encapsulated CANPs (114, 115).

4.5.2. Transmission electron microscope (TEM)

Transmission electron microscope was used to confirm the size measurements and gain insight into the morphology of the NPs. The morphological analysis of blank CANPs and DOX encapsulated CANPs were performed by a Tecnai F20 microscope (200 keV) at the Electron Microscope Unit, Department of Physics at the University of the Western Cape. A small amount of the synthesized CANPs solution was dropped on the copper mesh, adsorbed it for 5 min, and, after natural drying, covered the

copper mesh on 2% phosphotungstic acid dyeing solution, dyed it for 10 s, absorbed phosphotungstic acid with filter paper, and then applied 80 kV accelerating voltage for analysis and image scanning. The same was conducted for DOX encapsulated CANPs using a slightly modified method by (116). The image analysis tool ImageJ software was used for analysis of the images to measure the NP size.

4.5.3 Scanning Electron Microscope (SEM)

Prior to imaging, the freeze-dried CANP samples were mounted on aluminium stubs with double sided carbon tape. The samples were then coated with a thin (~10 nm thick) layer of gold, using a Leica EM ACE200 Gold Sputter Coater. This was done to make the sample surface electrically conductive to avoid electron build-up on the sample surface which can cause electron charge. Beam conditions during the quantitative analysis and backscattered electron image analysis on a Zeiss MERLIN were 20 kV accelerating voltage, 16nA probe current, with a working distance of 9.5 mm and a beam current of 11nA. The counting time was 10 seconds live-time. Gold was automatically excluded from analysis due to sample coating with gold (117).

4.5.4. Doxorubicin encapsulation efficiency

Determining DOX encapsulation efficacy (EE %) by UV

Preparation of doxorubicin standard samples

The stock solution was prepared by dissolving 1 mg DOX in 1ml of deionized water. A two-fold serial dilution from the stock solution was done to achieve the following concentration range: 0.005,0.01, 0.021, 0.063, 0.125, 0.25, 0.5,1 mg/ml (n=3).

Doxorubicin quantification: determining EE %

The indirect method was utilized to calculate doxorubicin encapsulated in the CANPs. DOX encapsulated CANPs were centrifuged (18 000 x g for 30 minutes) and the supernatant was analyzed for doxorubicin concentration (UV-Vis, 480 nm wavelength (n=3)). The DOX concentration was determined using the linear calibration curve and the EE (%) was calculated by the following equation.

$$\%EE = \frac{\text{Mass of drug used for formulation} - \text{mass of free drug}}{\text{mass of drug used for the formulation}} \times 100 \dots \dots \dots \text{equation 1}$$

4.5.5. Fourier Transform Infrared Spectroscopy

The surface chemical properties of DOX encapsulated CANPs were studied by FTIR (118). This was used to identify the functional group compounds that are on the surface of the NPs. To evaluate DOX, ALG, CS, lyophilized CANPs and DOX encapsulated CANPs, a small amount of each sample was weighed and 300 mg of potassium bromide, respectively, and grinded evenly together. The sample was dried in an infrared dryer and then pressed under 20 MPa for 5 min to obtain the sample to be tested. Each of the sample measured was scanned in the wavenumber range of 4000~400 cm⁻¹ to obtain the corresponding spectrogram, and the infrared absorption peaks of each sample was compared and analyzed, respectively using a slightly modified method by (116).

4.6. Statistical analysis

Data was collected in an Excel sheet and analyzed as a mean ± standard deviation, while IC₅₀ values were calculated using the GraphPad statistical program (Version 8). One-way analysis of variance (ANOVA) was used, followed by Tukey's post hoc test for multiple comparisons. Significance level was set at alpha 0.05.

4.7. RESULTS AND DISCUSSION

4.7.1. Synthesis of Chitosan alginate nanoparticles by ionotropic gelation

CANPs were successfully synthesized using the ionotropic gelation method which is based on the capability of polyelectrolytes to crosslink in the presence of counter ions (119). It is a two-step procedure based on the ionotropic gelation of polyanion with calcium chloride followed by polycationic crosslinking as shown in Figure 4.2. CaCl_2 was first added to an ALG solution, and then the CS solution (120). The guluronate residues in alginate interact with calcium ions to form a gel, it is known that higher G block concentrations in ALG result in stronger interactions. The CANPs were created by interacting negative carboxylic acid groups on ALG strands with positive amine groups on CS polymers (72). Since both ALG and CS are pH-sensitive polymers, their charges at various pH levels would significantly affect the formation and properties of CANPs. In an acidic environment, ALG has a low water solubility, and CS has a low water solubility at neutral or alkaline pH (17).

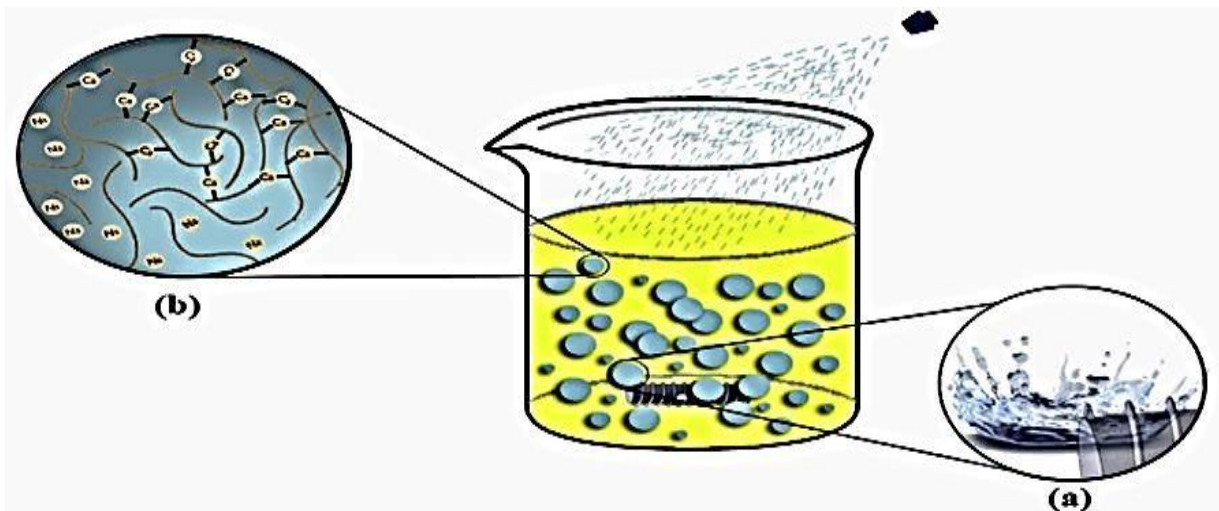


Figure 4. 2: Gelation procedure diagram; (a) shrinkage of sodium alginate; (b) crosslinking with calcium ions (121).

4.7.1. Characterization of the synthesized blank CANPs using DLS

DLS is a standard analytical method used to examine particle sizes and size distributions with diameters ranging from a few nanometres to a few microns (122). The blank nanoparticle hydrodynamic diameters, PDI and zeta potentials were determined after washing using DLS and Zetasizer as shown in Table 4.1. The ratios were established using a fixed concentration of ALG (0.06%) and varying concentrations of the CS (0.02%, 0.05%, 0.08% w/v) and Ca (0.04%, 0.067%, 0.1% w/v). This was all done at fixed ALG, CS and Ca volumes of 10 ml, 1.5 ml and 2 ml, respectively.

Table 4. 1: Hydrodynamic diameter, polydispersity index (PDI) and zeta potential of ALG-Ca-Cs NPs. Data are provided as mean \pm S.D. (n = 3).

Formulation	% w/v			Size	PDI	ZP (mV)
	ALG	CS	Ca			
A1`	0.06	0.02	0.04	279.44 \pm 5.79	0.428 \pm 0.02	-25.20 \pm 3.54
A2	0.06	0.02	0.067	319.22 \pm 4.56	0.487 \pm 0.05	-23.69 \pm 0.51
A3	0.06	0.02	0.1	356.23 \pm 24.69	0.540 \pm 0.02	-19.29 \pm 1.67
B1	0.06	0.05	0.04	362.73 \pm 12.83	0.442 \pm 0.03	-24.72 \pm 2.31
B2	0.06	0.05	0.067	447.43 \pm 8.95	0.461 \pm 0.03	-20.98 \pm 0.87
B3	0.06	0.05	0.1	491.44 \pm 33.66	0.840 \pm 0.09	-22.34 \pm 1.34
C1	0.06	0.08	0.04	374.04 \pm 11.35	0.393 \pm 0.08	-25.59 \pm 0.84
C2	0.06	0.08	0.067	463.80 \pm 4.258	0.334 \pm 0.03	-22.70 \pm 1.39
C3	0.06	0.08	0.1	535.70 \pm 39.62	0.330 \pm 0.03	-21.80 \pm 1.23

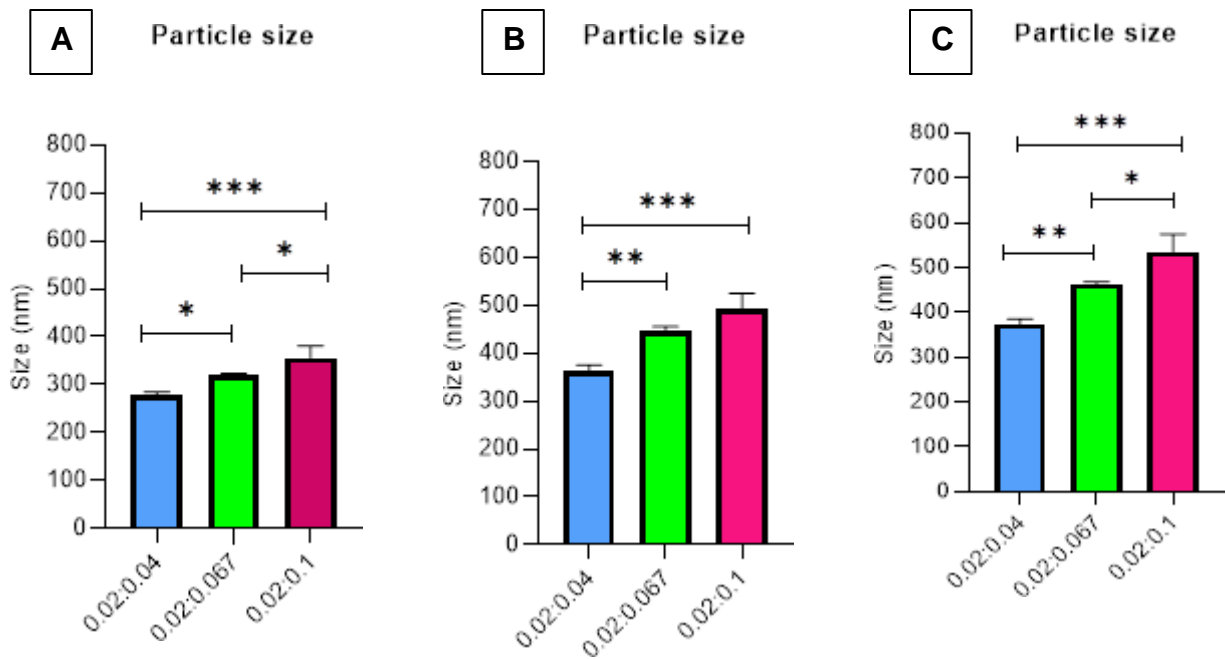


Figure 4. 3: Size comparisons of blank CANPs with varying ALG-CS-Ca mass ratios (n=3). (A) The results showed that there was a statistically significant difference amongst all the mass ratios. (B) The results showed that there was a statistically significant difference amongst the mass ratios except between 0.05:0.067 and 0.05:0.1 mass ratios. (C) The results showed that there was a statistically significant difference amongst all the mass ratios. Statistical significance was indicated by not significant (ns) (p-value > 0.05), *: significant (p-value ≤ 0.05), **: very significant (p-value ≤ 0.01), ***: extremely significant (p-value ≤ 0.001), ****: extremely significant (p-value ≤ 0.0001).

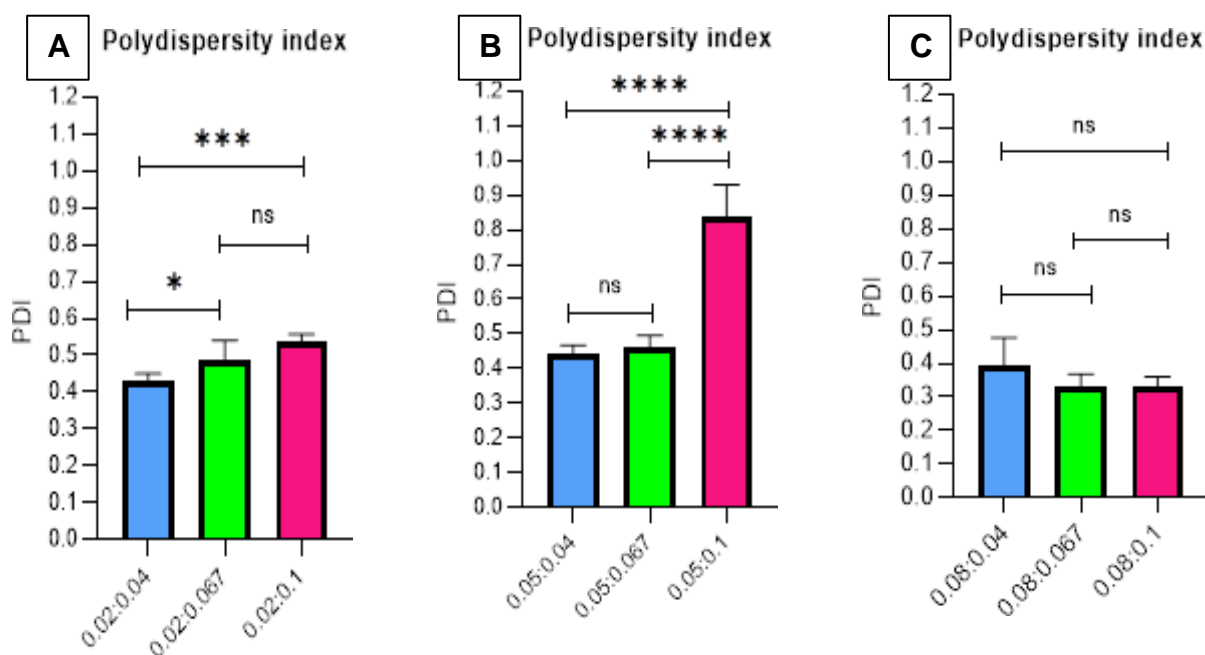


Figure 4. 4: PDI comparisons of blank CANPs with varying ALG-CS-Ca mass ratios (n=3). (A) The results showed that there was statistically significant difference amongst all the mass ratio except between 0.02:0.067 and 0.02:0.1 mass ratios. (B) The results showed that there was statistically significant difference amongst all the mass ratio except between 0.05:0.04 and 0.05:0.067 mass ratios. (C) The results showed that there was no statistically significant difference amongst all the mass ratios. Statistical significance was indicated by not significant (ns) (p-value > 0.05), *: significant (p-value ≤ 0.05), **: very significant (p-value ≤ 0.01), ***: extremely significant (p-value ≤ 0.001), ****: extremely significant (p-value ≤ 0.0001).

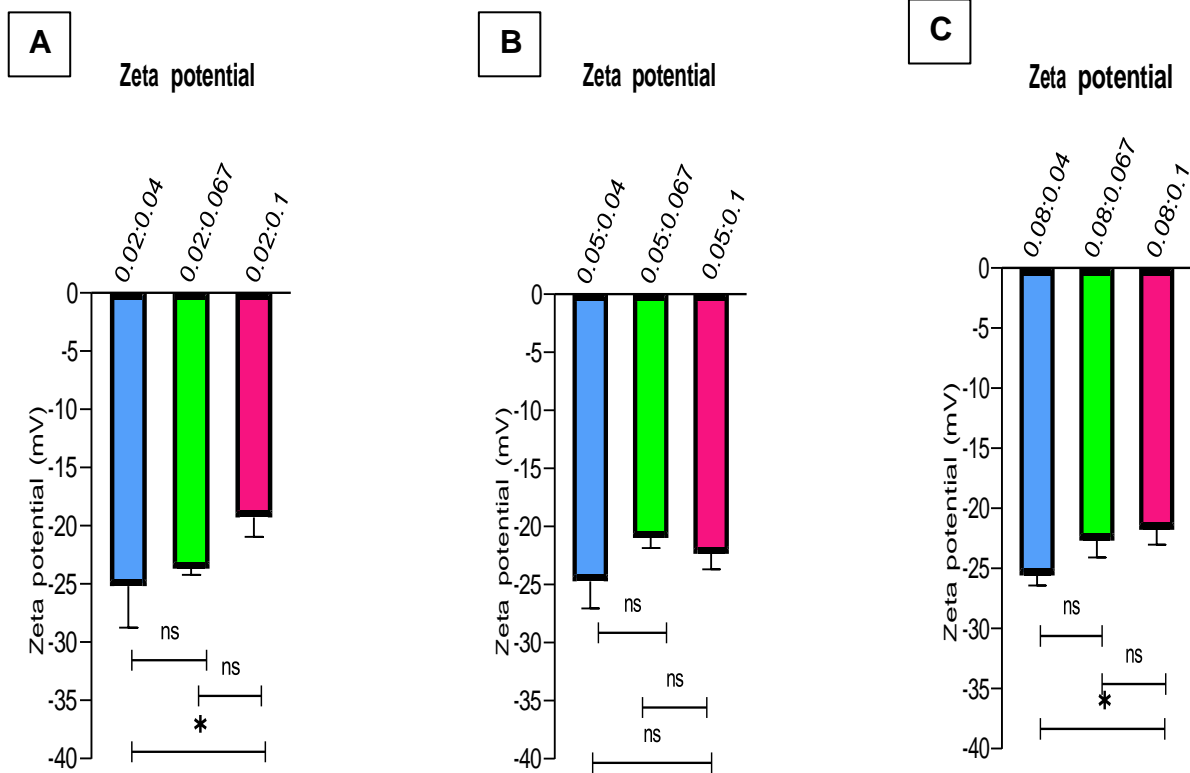


Figure 4. 5: Zeta potential comparisons of blank CANPs with varying ALG-CS-Ca mass ratios (n=3). (A) The results showed that there was no statistically significant difference amongst all the mass ratio except between 0.02:0.04 and 0.02:0.1 mass ratios. (B) The results showed that there was statistically significant difference amongst all the mass ratios. (C) The results showed that there was no statistically significant difference amongst all the mass ratios except between 0.08:0.04 and 0.08:0.1. Statistical significance was indicated by not significant (ns) (p-value > 0.05), *: significant (p-value ≤ 0.05), **: very significant (p-value ≤ 0.01), ***: extremely significant (p-value ≤ 0.001), ****: extremely significant (p-value ≤ 0.0001).

DLS was used to characterize sizes of the nine formulations of the blank CANPs. The average hydrodynamic diameter of formulation (A₁, A₂ and A₃) ranged from 279.44 ± 5.79 nm to 356.23 ± 24.69 nm, formulation (B₁, B₂ and B₃) ranged from 362.73 ± 12.83 nm to 491.44 ± 33.66 nm and formulation (C₁, C₂ and C₃) ranged from 374.04 ± 11.35 to 535.70 ± 39.62 nm as shown in the Table 4.1 and Figure 4.3. Formulation A₁ had the smallest size and C₃ had the largest size. Statistical analysis showed significant difference amongst the A₁, A₂ and A₃ formulations as shown in Figure 4.3, suggesting that various ratios of CaCl₂ significantly affected the CANP size. The results also showed that there was a statistically significant difference amongst the mass ratios except between 0.05:0.067 and 0.05:0.1 mass ratios. The results also showed that there was a statistically significant difference amongst all the mass ratios. This is not surprising as measurements are taken in water and chitosan NPs have been shown to swell rapidly in this setting (123, 124). (125) reported a mean hydrodynamic diameter of 303 nm which is the range of the CANP sizes obtained in this study. However, (126) reported that the average size for CANPs was 119.5 ± 49.9 nm which is smaller than the sizes obtained in this study.

The polydispersity index (PDI) describes the distribution or dispersion of NPs with a range between 0 and 1 (127). The PDI value was used to reflect the nanoparticle size distribution (128). NPs with PDI value < 0.1 is considered as highly monodisperse, while those with a PDI value of 0.1 - 0.4 are considered to have a moderately disperse distribution and those > 0.4 are highly polydisperse (129). The average PDI of formulation (A₁, A₂ and A₃) ranged from 0.428 ± 0.02 to 0.540 ± 0.02, formulation (B₁, B₂ and B₃) ranged from 0.442 ± 0.03 to 0.840 ± 0.09 and formulation (C₁, C₂ and C₃) ranged from 0.393 ± 0.08 to 0.330 ± 0.03 as shown in the Table 4.1 and Figure 4.4.

Zeta potential indicates whether samples will have a good colloidal stability, where particles with zeta potentials above +30 mV or below -30 mV usually considered as being stable. The average zeta potential of formulation (A₁, A₂ and A₃) ranged from -25.20 ± 3.54 mV to -19.29 ±1.67 mV, formulation (B₁, B₂ and B₃) ranged from -24.72±2.31 mV to -22.34 ±1.34 mV and formulation (C₁, C₂ and C₃) ranged from -25.59 ±0.84 mV to -21.80 ±1.23 mV as shown in Table 4.1 and Figure 4.5. The presence of carboxylic acids on the ALG chains imparted a negative surface charge. (15) suggested that when utilizing NPs for drug administration, positively charged surfaces provide an extra benefit since they can move more easily through negative channels in the cell membrane. The results contradict with the findings of (130), that the zeta potential of the CANPs ranges between +16.2 and +40.3 mV, which showed a dependency on the concentration of CS. They reported that the gradual increase in the zeta potential was noted with the increase in CS concentration and the reduction in ALG concentration. However, the results agree with the negative zeta potentials findings of (131), that reported that the zeta potential of CANPs ranged from -17.2 to -29.2 mV.

4.7.2. Encapsulation of DOX in CANPs

The size of formulation A₁ was the final determinant for the optimum ratio, despite obtaining desirable PDI and ZP readings for the on other formulations. Once the size (279.44 ± 5.79 nm), PDI (0.428 ±0.020) and zeta potential (-25.20 ± 3.54mV) of CANPs were optimised, DOX was encapsulated.

DOX's limited therapeutic index might be expanded by being encapsulated in NP, allowing for a sustained release of the substance over time. As the theoretical

maximum amount of the medicine is never in circulation at once, this may help to reduce toxicity (132). Liposomal doxorubicin (Doxil®), which the FDA approved in 1995 for Kaposi's sarcoma, is the most well-known method of encapsulating DOX. Despite liposomal DOX's demonstrated therapeutic superiority and enhanced tolerability, specific side effects appeared after therapy (133).

Different concentrations of DOX were tested using a constant ratio of alginate: chitosan. Encapsulation efficiency of each concentration of DOX was calculated and compared, as well as the particle size, PDI and zeta potential as shown in Table 4.2. The average hydrodynamic diameter of the DOX-CANPs ranged from 298.6 ± 38.10 nm to 761.4 ± 57.91 nm. The sizes of the blank CANPs are slightly smaller than the DOX encapsulated CANPs. The results revealed that there was an increase in particle size after the encapsulation of DOX. The size of the NPs decreased as the concentration of DOX increased. However, these findings contradict the results of (15) who found no change in the NPs size after encapsulation of DOX in CANPs. The average PDI of the DOX-CANPs ranged from 0.359 ± 0.10 to 0.900 ± 0.14 . The average zeta potential of the DOX-CANPs ranged from -21.77 ± 5.11 mV to -26.34 ± 1.20 mV. The difference between the encapsulated and blank NPs is considered as indication for the interaction with doxorubicin (79). The findings contradict the results of (15) that reported DOX encapsulated CANPs have a positive zeta potential (+35 mV), a mean particle size of 100 nm, and a high EE% (95%).

4.7.3. Establishing the standard curve for doxorubicin

A standard curve was established as a factor of the absorbance of DOX relative to its concentration. The standard curve was utilized in characterizing the quantity of DOX incorporated in CANPs. The standard curve generated for DOX showed high

regression coefficient of 0.9977 with a linear regression equation of $Y = 3.442X - 0.03542$ as shown in Figure 4.6. The mean slope was 3.277 to 3.608 and the y-intercept when $x = 0$ was -0.1030 to 0.03212 whereas the x-intercept when $y=0$ was -0.009617 to 0.02909.

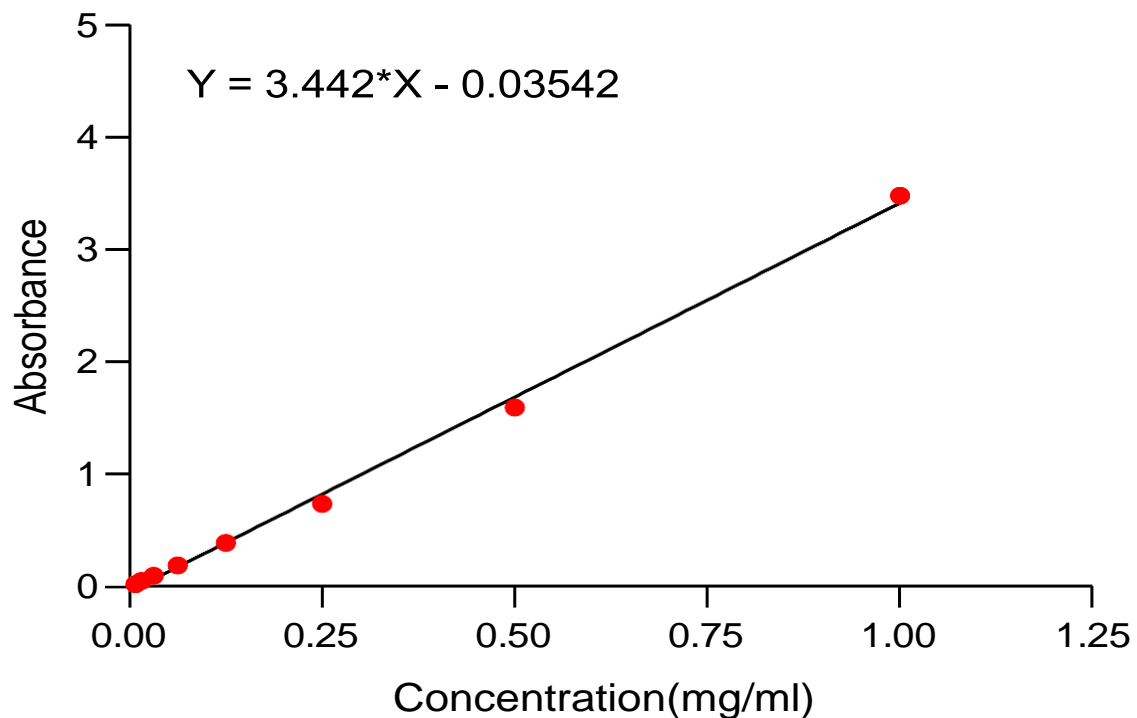


Figure 4. 6: Standard curve generated for DOX, absorbance versus concentration (range 0.008 -1mg/ml), DI water measured at 480 nm wavelength. Data representation; n=3; mean \pm SD.

Determining EE (%)

The amount of DOX encapsulated in CANPs was measured using the indirect method. This involved determining the DOX concentration in the aqueous supernatant of DOX encapsulated CANPs. The EE (%) was calculated from the absorbance value of the

sample supernatant using the linear regression equation $Y = 3.442X - 0.03542$ based on the standard curve. There was no linear relationship in EE (%) and concentration of DOX. Concentration of DOX with the highest EE (%) was 0.06 mg/ml and the one with lowest was 0.005 mg/ml. The highest EE (%) was 15.97% and the lowest was 11.63%. However, these findings contradict the results of (110) who found a linear relationship between concentration of DOX and EE %, it reported an increased EE% from 67% to 80% with the enhancement of drug/carrier ratio from 1 mg/ml to 2 mg/ml.

Table 4. 2: Characterization of the synthesized DOX encapsulated CANPs

Concentration of DOX (mg/ml)	Size (nm)	PDI	ZP (mV)	EE (%)
0.06	298.6 ±38.10	0.359 ±0.10	-24.63 ±1.40	15.97
0.04	313.0 ± 16.07	0.585 ±0.10	-25.65 ±2.71	13.53
0.02	356.4 ±28.19	0.701 ±0.17	-23.90 ±1.98	13.57
0.01	392.1 ±45.04	0.714 ±0.17	-24.60 ±2.55	14.08
0.005	476.6 ±48.78	0.733 ±0.02	-26.34 ±1.20	11.63
0.0025	633.2 ±0.64	0.850 ±0.16	-25.34 ±2.02	13.88
0.00125	633.8 ±10.32	0.716 ±0.11	-21.77 ±5.11	15.18
0.000625	761.4 ±57.91	0.900 ±0.14	-22.83 ±1.16	14.81

4.7.4. HIGH RESOLUTION TRANSMISSION ELECTRON MICROSCOPY

The morphological and elemental composition of the nanoparticles were analysed through higher resolution transmission electron microscope (HRTEM). The NPs morphology was evaluated using TEM and the results are illustrated in figure 4.7 and 4.8 for both blank and the DOX encapsulated CANPs, respectively. The blank CANPs appeared to be spherical NPs, although a tendency for these particles to agglomerate was observed. The measured average diameter of these particles was 80 - 90 nm

(n=15) for both blank and loaded nanoparticles as illustrated in the size distribution diagram. A study by (134) had shown the particle sizes of CANPs obtained from TEM to be around 63 nm. Thus, using the above-mentioned method we were able to obtain larger CANPs. These observations were consistent with the study by (135) indicating that nanoparticle sizes measured by TEM are smaller than those of DLS. This could be because, DLS measurements give the hydrodynamic diameter of NPs in suspension, while TEM images are obtained from samples after freeze or oven drying. In addition, particle size differences can also be a result of the multiple scattering effect in the DLS technique; multiple scattering refers to the process when light scattered by the diffusing particle is re-scattered by one or more particles before reaching the detector (136). The TEM images of CANPs in (131) study indicated that the optimized NPs are well dispersed as individual particles with a spherical and uniform shape.

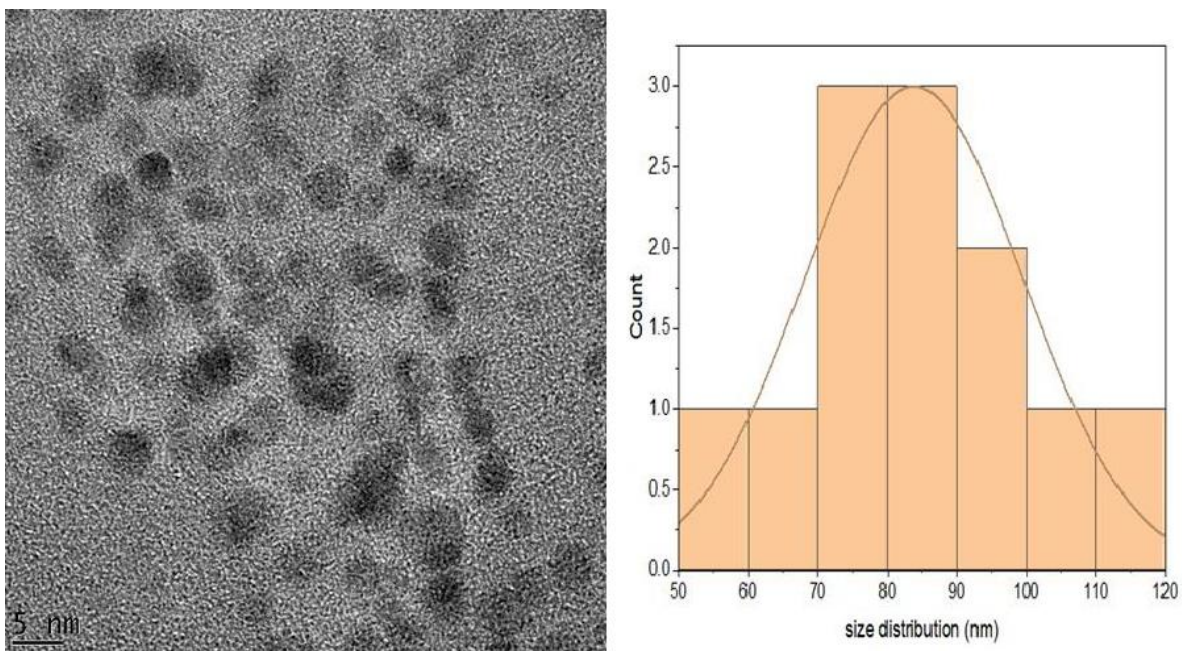


Figure 4. 7: The transmission electron microscope (TEM) image and size distribution for blank CANPs.

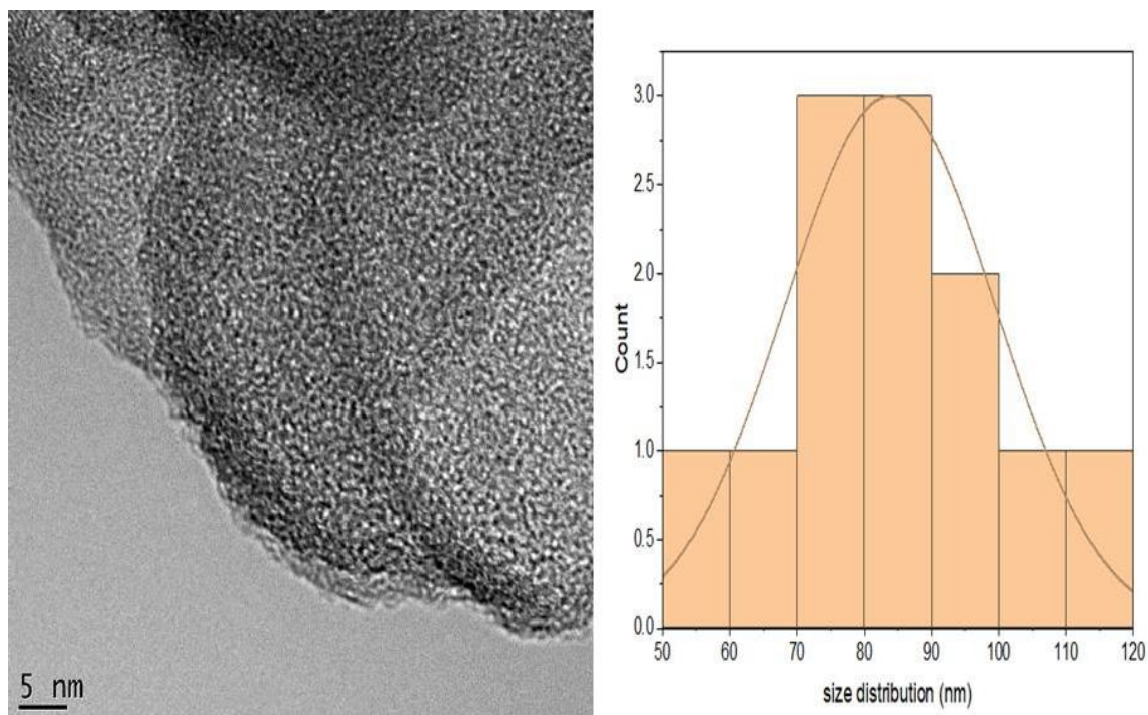


Figure 4. 8: The transmission electron microscope (TEM) image and size distribution of DOX encapsulated CANPs.

4.7.5. Scanning electron microscopy of the CANPs

SEM results illustrated that the blank (formulation A1) and DOX-encapsulated CANPs formed aggregates and had inconsistent spherical shapes. After synthesis, the NPs were lyophilized, and the powder was examined. SEM analysis revealed a rough, grainy appearance on the surface of the powder as shown in Figure 4.9, and the presence of aggregated, poorly defined NPs. The images suggest that upon lyophilization, the NP matrix was disrupted and the electrostatic bonds between the polymers collapsed, causing a grainy, flocculated appearance (137, 138). Both the blank and DOX-encapsulated CANP also showed surface cracks probably caused by partial collapsing of the polymer network during drying (139). The SEM micrograph of CANPs in (140) study reveals a spherical or sphere-like morphology and for the

encapsulated CANPs, a distinctly bigger and agglomerated morphology was observed.

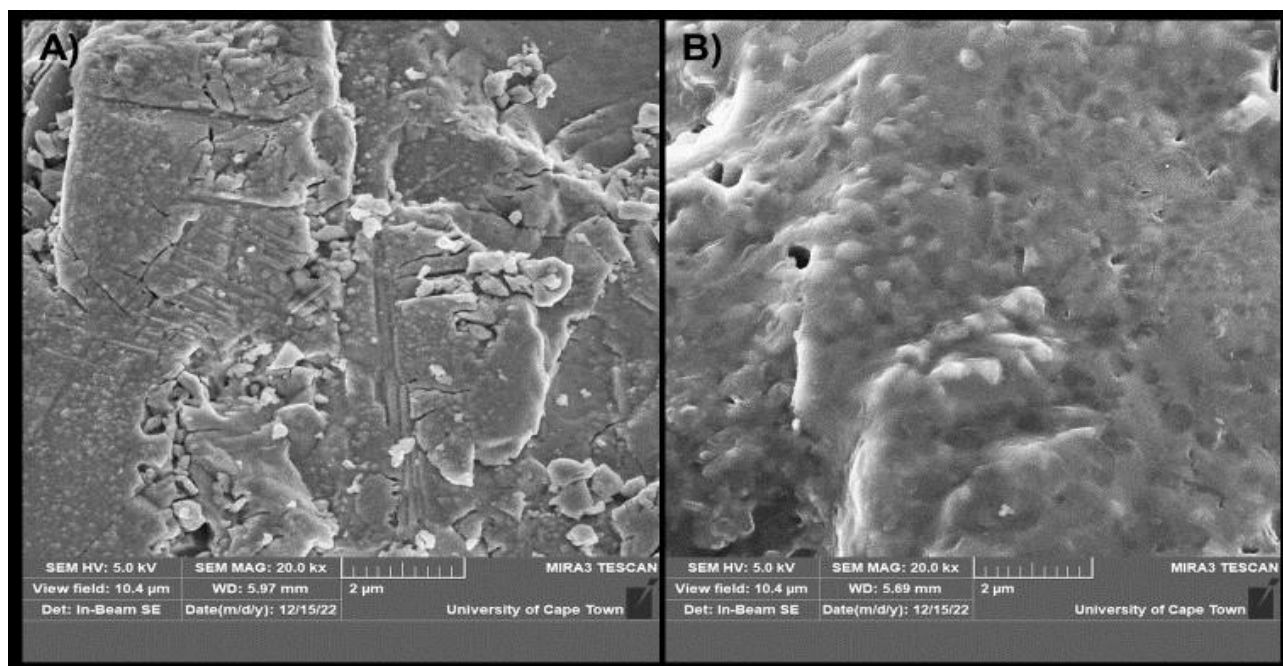


Figure 4. 9: The scanning electron microscope (SEM) image of (a) blank CANPs and (b)DOX encapsulated CANPs.

4.7.6. FTIR

The successful encapsulation of doxorubicin into the chitosan-alginate nanoparticles was confirmed by FTIR (80). It was used to generate spectra for ALG, CS, DOX, CANP and DOX-CANP as illustrated in Figure 4.10. Absorptions from 4000 to 400 cm^{-1} in the fingerprint region are assigned to the bending of metal to oxygen and/or hydrogen bonds. The result showed that numerous peaks were detected, which may indicate that DOX-CANP is complex structure material. The CS spectrum exhibited a narrow absorption peak at 3614 cm^{-1} which was assigned to the -OH (hydroxide) bond. No other peaks between 3000 and 3200 cm^{-1} were found, informing there is no aromatic structure in all the spectrums. The ALG spectrum exhibited narrow absorption peaks at

3564 and 3422 cm^{-1} which were assigned to the -OH (hydroxide) bond, while that at 3114 cm^{-1} was assigned to a C-H group. DOX spectrum exhibited narrow absorption peaks at 3532 and 3320 cm^{-1} which were assigned to the -OH (hydroxide) bond, while that at 2894 was assigned to a C-H group. The CANP spectrum exhibited narrow absorption peaks at 3532 and 3320 cm^{-1} which were assigned to the -OH (hydroxide) bond, while those at the DOX-CANP spectrum exhibited narrow absorption peaks at 3532 and 3420 cm^{-1} which were assigned to the -OH (hydroxide) bond. No specific peak for aldehyde has been found at between 2700 and 2800 cm^{-1} . No triple bond region (2000 - 2500 cm^{-1}) was detected, informing no $\text{C}\equiv\text{C}$ bond in the materials. DOX-CANP shows some combination of peaks (A,B and C) from both DOX and CANP, which could be indicative of the encapsulation (141).

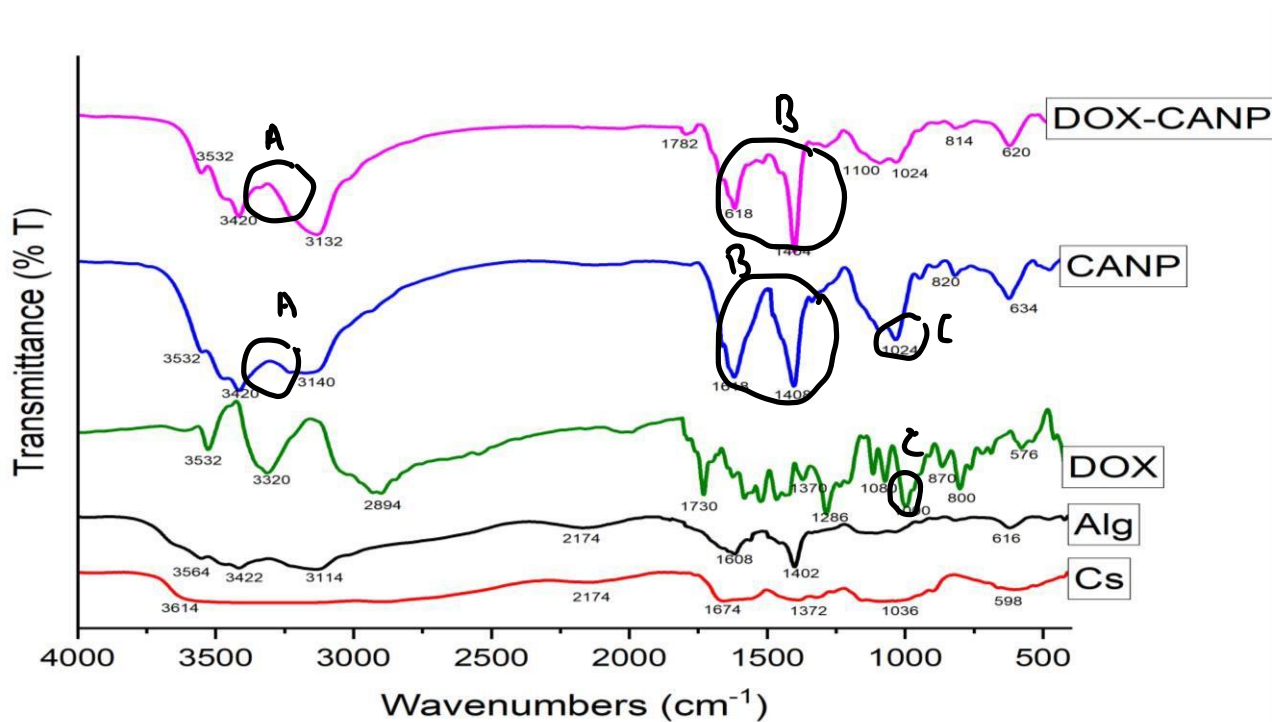


Figure 4. 10: FTIR spectra of alginate(black), chitosan (red), empty CANPs (blue), DOX loaded CANPs (green) and pure DOX (purple) registered in KBr pellets

CHAPTER 5: *IN VITRO* CYTOTOXICITY STUDIES

5.1. Introduction

This chapter describes the *in vitro* analysis of the DOX encapsulated CANPs effect on multidrug-resistant colon cancer cells using the MTT [3-(4,5-Dimethylthiazol-2-yl)-2,5-Diphenyltetrazolium Bromide] colorimetric assay. MTT assay is a colorimetric assay for assessing cell viability. The viable cells reduce the yellow tetrazolium dye MTT [3-(4, 5-dimethylthiazol-2-yl)-2, 5-diphenyltetrazolium bromide] to insoluble formazan crystals, which are purple in color (142). The cells were exposed to the free DOX, blank CANPs and the DOX encapsulated CANPs with and without CUR for 24 hours.

5.1.1. Aims and objective

The aim of this part of the study was to evaluate the cytotoxicity of blank and DOX encapsulated CANPs on Caco-2 cell line. The objective of this part of the study was to determine the cytotoxicity effects of DOX encapsulated CANPs and CUR on the multidrug-resistant cancer cell lines using MTT assay.

5.2. Materials and reagent

Apparatus

All laboratory work was performed in a sterile environment under laminar flow (Labotec, South Africa). A humidified, 5% CO₂ incubator (Marshall Scientific, USA) was used as a growing environment for the cells with the temperature set at 37°C. A Digicen 21 centrifuge (Ortoarlresa, Spain) was be used for centrifuging to obtain cell pellets. The cell Countess™ automated cell counter was used for cell counting.

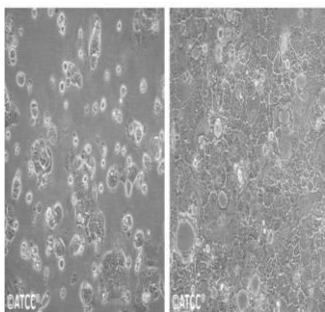
Chemicals and reagents

Dimethyl Sulfoxide (DMSO) (Sigma-Aldrich, USA), Phosphate Buffer Saline (PBS) (Sigma-Aldrich, USA), Trypsin-ethylenediaminetetraacetic acid (EDTA) (0.25%) (Sigma-Aldrich, USA), Doxorubicin, and 3-(4,5-dimethylthiazol-2-yl)-2,5-diphenyltetrazolium bromide (MTT) assay (Sigma-Aldrich, USA), Dulbecco's Modified Eagle's medium (DMEM) (Sigma-Aldrich, USA), Fetal Bovine Serum (FBS) (Sigma-Aldrich, USA), T25 tissue culture flask (Sigma-Aldrich, USA) and the water was obtained from a Barnstead EasyPure (II) UV-ultrapure water system (Thermo Fisher Scientific, USA). All other chemicals and reagents used were of analytical grade.

Cell lines and the culture media

The human colon cancer cell line Caco-2 (ATCC® HTB-37™) were acquired from the American Type Culture Collection (ATCC) (Manassas, VA, USA). The table below summarizes the cell line used in this study with their main characteristics (ATCC, assessed on 22/02/2022).

Table 5. 1: General information on the selected colon cell line

Cell type	Tissue	Morphology	Disease	Expression of ABC transporters
Caco-2	Colon		Colorectal adenocarcinoma	P-gp and MRP-1

5.3. Methods

5.3.1. Cell culture

Dulbecco's Modified Eagle's medium (DMEM) was used to maintain the Caco-2 cell line. All cell lines were supplemented with 10% FBS and grown at 37°C in a humidified incubator set at 5% CO₂. After they had reached an 80 -100% confluent monolayer, the media was aspirated from the flask. The cells were washed with phosphate buffered saline (PBS) prior to the addition of 0.25% (w/v) trypsin 0.53 mM EDTA for 3 minutes at 37°C. Subsequently, an equal volume of serum-containing medium was added to neutralise the trypsin. Cells were then centrifuged at 30 000 rpm for 5 minutes and washed with PBS prior to resuspension in medium.

5.3.2. Preparations

Drug preparation

DOX was used as the positive control. The initial stock solutions of 1 mg/ml were prepared with distilled water. The solutions were evaluated at eight concentrations that range from 0.000625 -0.06 mg/ml.

5.3.3. Counting cells using a Cell Countess™ automated cell counter

The confluent cells were harvested through trypsinization, which involved aspiration of the media from the flask and washing the cells with 2 ml of DPBS to remove dead cell debris. 1 ml of 0.25% trypsin-EDTA was added, followed by gentle swirling of the flask and incubation at 37°C for 3 minutes, to detach the cells from the flask surface. Thereafter, 3ml of complete medium was added to inactivate/neutralize the trypsin and 2ml of DPBS to wash-off the remaining cells. The cells were centrifuged at 30 000 rpm for 5 minutes at 25°C. Cells were then counted using a cell counter. The cell

suspension (10µl) was diluted by adding an equal volume of trypan blue dye. About 10µl of the coloured suspension was placed into the counting chamber. Here, viable cells remained uncoloured whereas the non-viable cells absorbed the blue dye. The viable cell density was adjusted to 100 000 cells/100 µl per. 100µl of the cell suspension together with a 100µl of the complete growth medium were added to all the wells in the plate, except for well A1, which contained complete growth medium only and served as a blank. Thereafter the plate was incubated, and the cells were allowed to adhere for 24 hours. Following the 24-hour incubation, the cells were exposed to different test substances as described in Section 5.3.4

5.3.4. Cytotoxicity on the colon cell lines.

Cells were seeded in a 96-well flat-bottom plate at a density of 100 000 cells/well. The cells were then incubated for 24 h at 37°C with 5% CO₂ to allow for attachment to the bottom of the wells. After incubation, the cells were exposed to 50µl/well of the different concentrations of the DOX encapsulated CANPs (0.000625 -0.06 mg/ml) and positive controls (0.000625 -0.06 mg/ml) for a treatment period of 24 h. The preparation of the samples in a 96-well plate is illustrated in Table 3.1. After the designated duration of 24 h of drug exposure, MTT (0.5 mg/ml) was added to the plates and incubated for 2-4 h at 37 °C in 5% CO₂. Approximately 150 µl of the medium will be removed and the reduced formazan crystals was dissolved in 100 µl DMSO by incubation at room temperature for 30 min in the dark. The absorbance (optical density) of the color reaction was read at a wavelength of 570 nm utilizing an absorbance plate reader. The percentage of cell viability and fifty percent inhibitory concentrations (IC₅₀ values) was calculated. Each experiment was carried out three times (n=3) and analyzed in triplicates.

Table 5. 2: Experimental design

Treatment	Description
Negative control	Blank CANP
Positive control	DOX
Treatment 1	DOX encapsulated CANP
Treatment 2	DOX encapsulated CANP +CUR

Table 5. 3: Plate layout for the cytotoxicity experiment

	1	2	3	4	5	6	7	8	9	10	11	12	
A	BLANK	Untreated cells	DOX	CANP	0.06 mg/ml DOX - CANP	0.04 mg/ml DOX - CANP	0.02 mg/ml DOX - CANP	0.01 mg/ml DOX - CANP	0.005 mg/ml DOX - CANP	0.0025 mg/ml DOX - CANP	0.00125 mg/ml DOX - CANP	0.000625 mg/ml DOX - CANP	Untreated cells
B													
C													
D													
E													
F													
G													

5.3.4.1. Antiproliferation assay

The MTT colorimetric assay was performed with slight modifications as previously described by (94), to determine the antiproliferative activity of doxorubicin and the DOX encapsulated chitosan alginate nanoparticles on the selected colon cancer cell line. The assay relies on the capacity of mitochondrial succinate dehydrogenase enzymes in living cells to reduce the yellow, water-soluble substrate, MTT, into an insoluble, coloured formazan product that can be measured spectrophotometrically (143, 144).

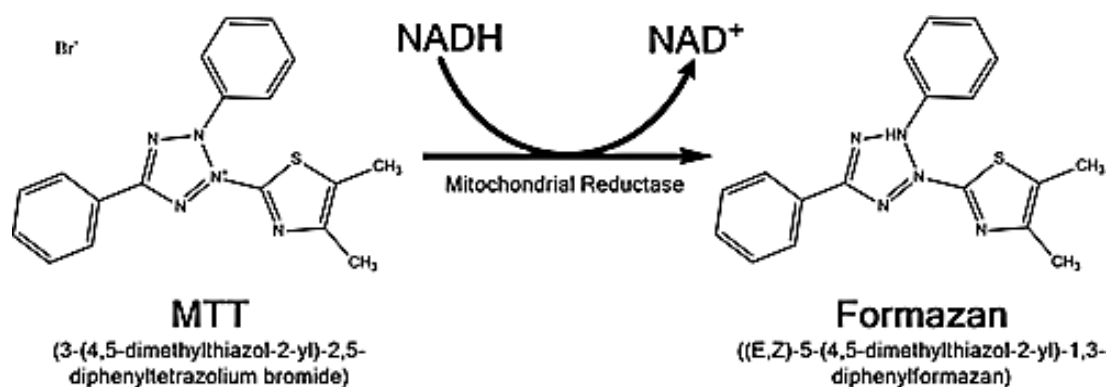


Figure 5. 1: Reduction of MTT to formazan crystals (143)

Reagent preparation

5 mg/ml of MTT solution was prepared by dissolving 5 mg MTT in 1 ml of DPBS. The solution was kept in a sterile light-protected container.

MTT assay

Following the 24-hour incubation, 20 μ l of MTT was added to each well and the plate was left to incubate for an additional 4 hours at 37°C in a CO₂ incubator. After incubation, the produced formazan salts produced appeared as dark crystals at the bottom of the wells. Thereafter, 100 μ l of DPBS was added to wash off the MTT and an equal amount of DMSO was added to each well to solubilize the formed formazan crystals, producing a purple solution and incubated for 30 minutes. The absorbance of each plate was measured using a microplate reader at a wavelength of 570 nm. The absorbance readings obtained showed the cell viability. Absorbance values greater than the cell control indicate cell proliferation, while lower values suggest cell death or inhibition of proliferation. The absorbance readings of the blank were subtracted from all samples, and readings from test samples were divided by those of the control and multiplied by a 100 to give percentage cell viability. The half-maximal inhibitory concentration (IC₅₀) values were extrapolated from a dose-response graph.

5.3.5. Combination studies

5.3.5.1. Curcumin (CUR) preparation

1 mg/ml of CUR solution was prepared by dissolving 1 mg of CUR in 1 ml of deionized water.

The purpose of the combination treatment is to evaluate the drug potentiating and sensitizing effect of the DOX encapsulated CANPs and CUR on MDR colon cancer

cell lines, respectively. The resistant colon cancer cell lines (Caco-2) were plated as explained in section 3.2.2.1. After 24 h, the cells were incubated with different

concentrations of DOX (60-0.625 µg/ml) and 25 µl of the DOX encapsulated CANPs and of CUR. The culture medium was used as controls. After 24 h incubation, the experiment will be completed by the addition of MTT, and measurement of the absorbance as explained in section 3.2.2.2.5. The percentage of cell viability and 50% inhibitory concentrations (IC₅₀ values) will be calculated. The inhibition of cell growth were calculated by the following equation.

The standard graph was plotted by taking a concentration of the drug in the X-axis and relative % inhibition in Y-axis.

$$\text{Cell viability} = \frac{[\text{test}]}{[\text{control}]} \times 100 \dots\dots\dots \text{equation 2}$$

Table 5. 4: Plate layout for the combination experiment

	1	2	3	4	5	6	7	8	9	10	11	12
A	BLANK	DOX (0.000625-0.06 mg/ml)	CANP	0.06 mg/ml DOX – CANP + CUR	0.04 mg/ml DOX – CANP + CUR	0.02 mg/ml DOX – CANP + CUR	0.01 mg/ml DOX – CANP + CUR	0.005 mg/ml DOX – CANP + CUR	0.0025 mg/ml DOX – CANP + CUR	0.00125 mg/ml DOX – CANP + CUR	0.000625 mg/ml DOX – -CANP + CUR	Untreated cells
B	Untreated cells											
C												
D												
E												
F												
G												
H												

5.4. STATISTICAL ANALYSIS

Data was collected in an Excel sheet and analyzed as a mean ± standard deviation, while IC₅₀ values were calculated using the GraphPad statistical program (Version 8) for windows (GraphPad Software Inc.). Cytotoxicity results were expressed as the percentage of cell viability compared to the untreated controls. ANOVA will be used to make comparisons across groups. Significance level will be set at alpha 0.05.

5.5. RESULTS AND DISCUSSION

MDR is a major clinical problem in which cancer cells develop resistance to a variety of anticancer drugs that are structurally and functionally distinct from the initial drug after being exposed to it, hence the development of combination therapies constitutes an effective strategy to inhibit cancer cells and prevent the emergence of drug resistance (145, 146). Drug efflux can be caused by either intrinsic or acquired resistance. Drug efflux is dependent on transporters found in the outer biomembrane of cancer cells (147). These transmembrane proteins are ABC transporters, which use the energy released by ATP hydrolysis to eliminate xenobiotics from cells into bile, urine, or faeces. As a result, the bioavailability of drugs is reduced (148).

5.5.1. Cytotoxicity on Caco-2 cells

To demonstrate efficacy of the CANPs against a colon cancer cell line, empty CANP, free DOX, and CANPs with encapsulated DOX were administered to Caco-2 cells. Cell viability after 24 h exposure to the treatment was determined using MTT reagent. MTT assay determines cytotoxicity of a compound by measuring changes in intracellular NADPH-dependent oxidoreductase activity (149, 150). The optical densities of the control wells, the mean of which is set to a survival rate of 100%, define the initial status of living cells. It is noteworthy that the cell viability percentage of untreated control cells remained high (144, 151).

The half-maximal (50%) inhibitory concentration (IC_{50}) value is defined as the concentration required for 50% reduction in cell growth and proliferation(152). IC_{50} can help understand the pharmacological and biological properties of a chemotherapeutic agent (153). The relationship between IC_{50} and cytotoxicity is inversely proportional because the lower the IC_{50} values, the greater the cytotoxic activity and vice-versa. It is ideal to get a low IC_{50} value for the

cancerous cell line and a high IC₅₀ value for the normal cell line. The IC₅₀ values DOX and DOX-CANPs were 0.00123 ± 0.0003 and 0.00061 ± 0.0016 mg/ml, respectively. The dose-response curves for the free DOX and the encapsulated DOX are similar as shown in Figure 5.1, indicating similar therapeutic response.

Table 5. 5: IC₅₀ values of the standard drug (DOX), DOX-CANPs and DOX-CANP + CUR on the Caco-2 cell line.

Treatment	IC ₅₀ ± SD (mg/ml)
DOX	0.00123 ± 0.0003
DOX-CANPs	0.00061 ± 0.0016

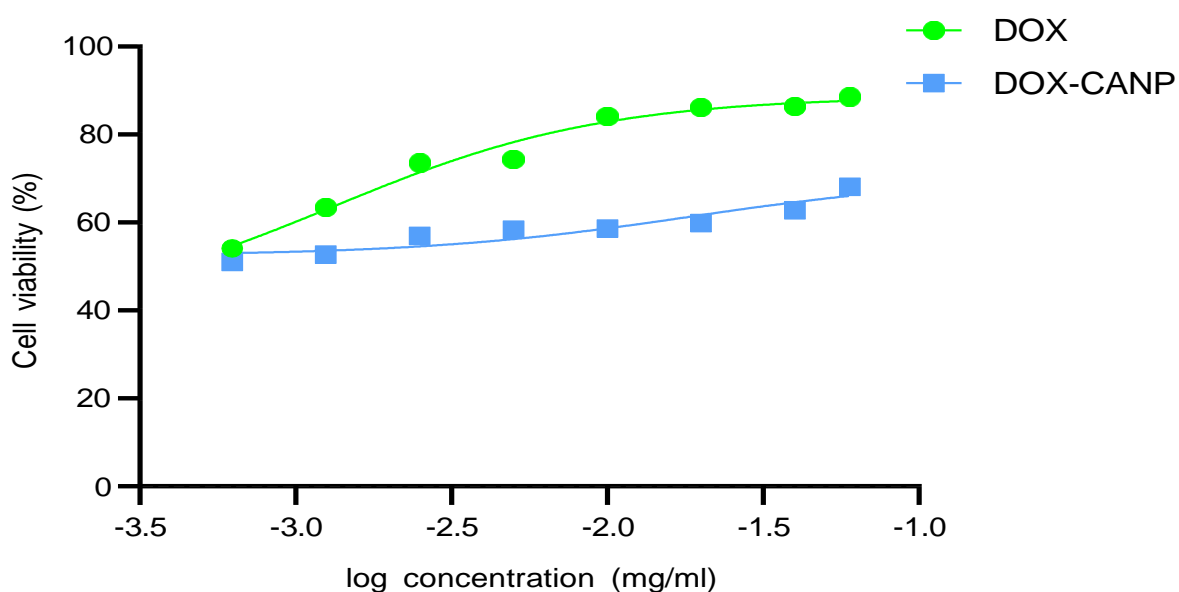


Figure 5. 2: Dose-response of Caco-2 cell line to various DOX and DOX-CANP after 24 hours of treatment. Cell survival was assessed via MTT (absorbance at 570 nm) assay. Results were reported as mean ± SD, n=3.

The cytotoxicity of the free DOX, DOX-CANP and CANP only against Caco-2 cells are illustrated in Figure 5.3. The results showed that there was statistically significant

difference between DOX and DOX-CANP in 0.06, 0.04, 0.02 and 0.01 mg/ml. The results also showed that there was no statistically significant difference in 0.005, 0.0025, 0.00125 and 0.000625 mg/ml. Lower concentrations of the free DOX and encapsulated DOX were more cytotoxic than at higher concentrations. This contradicts results reported by (150) where the cell viability systematically decreased with increasing DOX concentration.

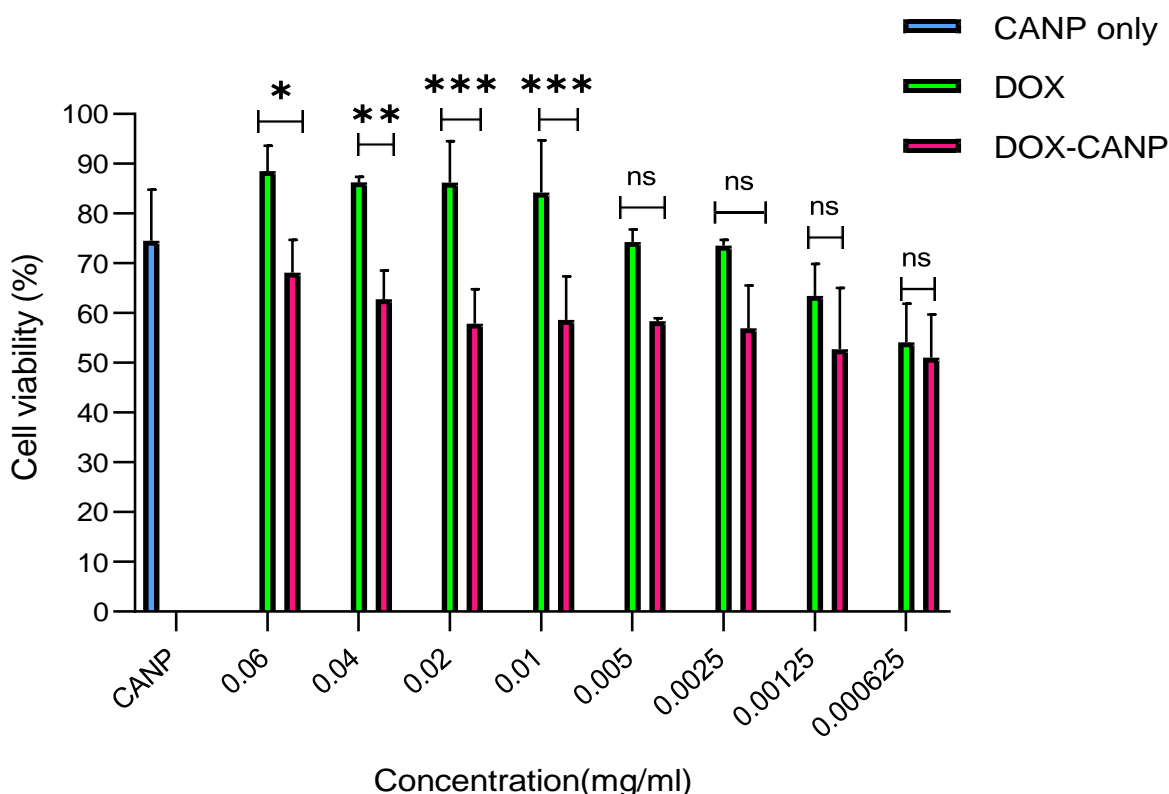


Figure 5. 3: Cytotoxicity of the free DOX, DOX CANP against Caco-2 cells after 24 hours of treatment. Cell survival was assessed via MTT (absorbance at 570 nm) assay. Results were reported as mean \pm SD, n=3. The results showed that there was statistically significant difference between DOX and DOX-CANP in 0.06,0.04,0.02 and 0.01 mg/ml. The results also showed that there was no statistically significant difference in 0.005,0.0025,0.00125 and 0.000625 mg/ml. Statistical significance was indicated by not significant (ns) (p-value > 0.05), *: significant (p-value \leq 0.05), **: very significant (p-value \leq 0.01), ***: extremely significant (p-value \leq 0.001), ****: extremely significant (p-value \leq 0.0001).

DOX is a commonly used anti-cancer anthracycline, but it has serious side effects, including dose-dependent and cumulative life-threatening cardiotoxicity and MDR development (154). These shortcomings have been tackled by entrapping DOX into NPs and using chemo-sensitizers (155). DOX-CANPs showed lower cell viability when compared to its free drug counterpart and CANPs alone. These CANPs may be of great interest for drug delivery purposes, as the side effects of the DOX would be reduced in systemic dosing of the encapsulated form. The encapsulation of DOX into the CANPs increased its efficacy against drug resistant cancer cells. For the DOX- CANPs to have a similar effect to that of the free drug, the encapsulated DOX must be present at a lower concentration. Contrary to the findings of (156), where a higher concentration of DOX was needed for DOX encapsulated nanoalginates show a similar effect to the free drug. The study reported that their findings were expected, as the encapsulated DOX is more hindered in its transport to the target site (156).

5.5.2. Effect of Curcumin and DOX-encapsulated CANPs on Caco-2 cells

Combination chemotherapy is a more effective way to treat cancer, compared to a single-agent treatment (157). CUR is a natural compound that inhibits the MDR protein family-member P-gp and blocks the transport of anti-cancer drugs out of cancer cells (158). It slows tumour growth, and research in recent years have shown that it can work in synergy with several chemotherapeutic treatments. However, the dosage form needs to be modified because this medication is poorly bioavailable and insoluble in water (159). The results showed that there was statistically significant difference between DOX-CANP and DOX-CANP + CUR in all the concentrations. The results show that combining the DOX-CANPs and CUR is more effective than DOX- CANPs alone. (160) showed that CUR reverses P-gp-mediated resistance

in drug resistant (SW620/Ad300) colon cancer cell line by enhancing the Dox-induced cytotoxicity and apoptosis (160). Cur also increases the efficacy of DOX-induced death in HCT-116 cells (161). It can be concluded that Cur may serve as a chemosensitizer for DOX. These results provide convincing evidence that combining curcumin with chemotherapy may be effective in overcoming drug resistance in colon cancer. The dose-response curves for the free DOX and the encapsulated DOX are similar as shown in Figure 5.4., indicating similar therapeutic response.

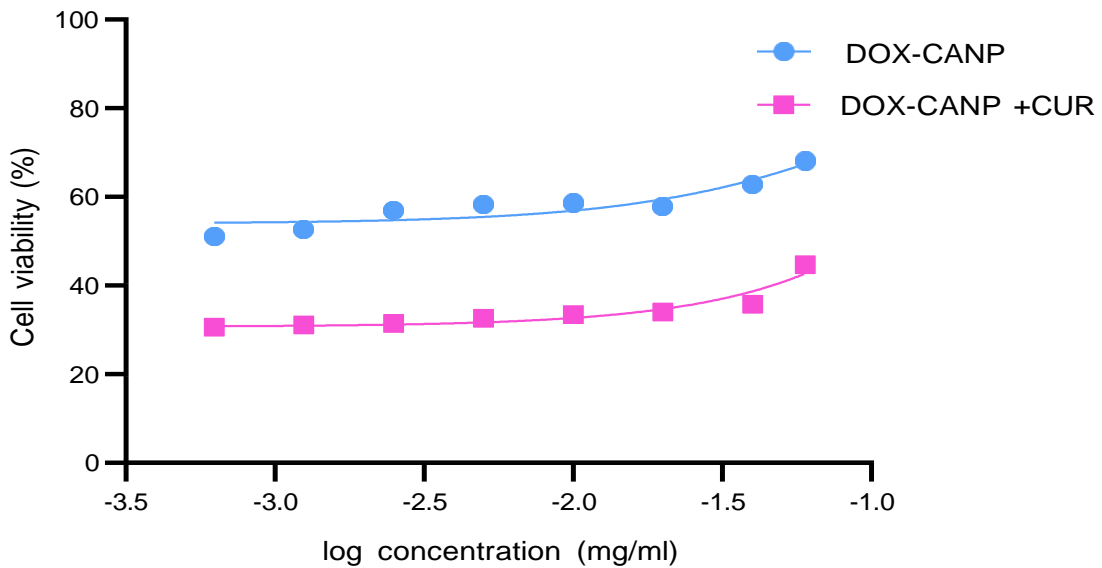


Figure 5. 4: Dose-response of Caco-2 cell line to various DOX-CANP and DOX-CANP +Cur after 24 hours of treatment. Cell survival was assessed via MTT (absorbance at 570 nm) assay. Results were reported as mean \pm SD, n=3.

The cytotoxicity of the DOX-CANP and DOX-CANP + Cur against Caco-2 cells is illustrated in figure 5.5.

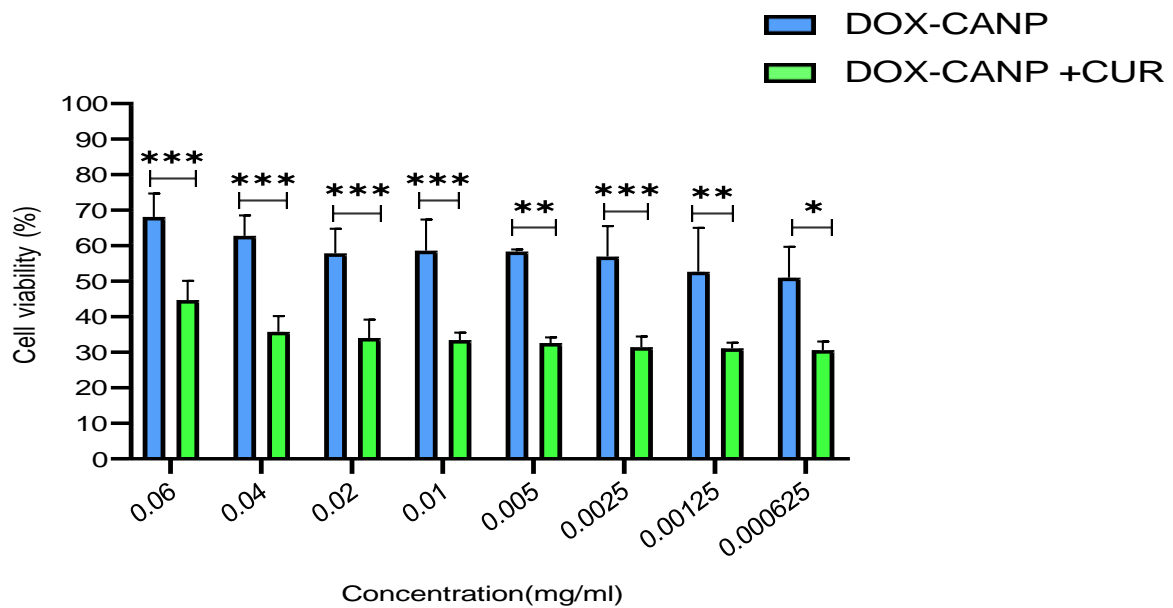


Figure 5. 5: Cytotoxicity of the DOX-CANP and DOX-CANP and curcumin against Caco-2 cells after 24 hours of treatments. Cell survival was assessed via MTT (absorbance at 570 nm) assay. The results showed that there was statistically significant difference between DOX-CANP and DOX-CANP + CUR in all the concentrations. Results were reported as mean \pm SD, n=3. Statistical significance was indicated by not significant (ns) (p-value > 0.05), *: significant (p-value \leq 0.05), **: very significant (p-value \leq 0.01), ***: extremely significant (p-value \leq 0.001), ****: extremely significant (p-value \leq 0.0001).

CHAPTER 6: CONCLUSIONS

MDR poses an enormous challenge in the management of cancer patients. This prevalent and adverse clinical problem frequently results in cancer recurrence and low survival rate. The overall aim of this study was to determine the potential of the co-delivery of DOX encapsulated CANPs and CUR as sensitizing agents in MDR colon cancer cell lines. Both the blank and DOX encapsulated CANPs were synthesized, characterized and evaluated for their cytotoxicity. DOX encapsulated CANPs decreased the cell viability of multidrug resistant colon cancer cell line (Caco-2). The results show that combining the DOX-CANPs and CUR is more effective than DOX-CANPs alone. CUR increases the efficacy of the DOX-CANPs against Caco-2 cell line.

Recommendations and limitations: Future studies should take into account the concentration of CANPs. Direct determination of the encapsulation efficacy using high performance liquid chromatography, for more direct evaluation than that observed in this present study. Future research for the validation of the DOX encapsulated CANPs and CUR for colon cancer treatment in vivo to better evaluate the safety, toxicity and efficacy.

CHAPTER 7: REFERENCES

1. Brand M, Gaylard P, Ramos J. Colorectal cancer in South Africa: An assessment of disease presentation, treatment pathways and 5-year survival. *South African Medical Journal*. 2018;108(2):118.
2. Sawicki T, Ruszkowska M, Danielewicz A, Niedźwiedzka E, Arłukowicz T, Przybyłowicz KE. A Review of Colorectal Cancer in Terms of Epidemiology, Risk Factors, Development, Symptoms and Diagnosis. *Cancers*. 2021;13(9):2025.
3. Rawla P, Sunkara T, Barsouk A. Epidemiology of colorectal cancer: incidence, mortality, survival, and risk factors. *Gastroenterology Review*. 2019;14(2):89-103.
4. Jansman FG, Postma MJ, Brouwers JR. Cost considerations in the treatment of colorectal cancer. *Pharmacoeconomics*. 2007;25:537-62.
5. Bukowski K, Kciuk M, Kontek R. Mechanisms of multidrug resistance in cancer chemotherapy. *International journal of molecular sciences*. 2020;21(9):3233.
6. Alakhova DY, Kabanov AV. Pluronic and MDR Reversal: An Update. *Molecular Pharmaceutics*. 2014;11(8):2566-78.
7. Xiao H, Zheng Y, Ma L, Tian L, Sun Q. Clinically-Relevant ABC Transporter for Anti-Cancer Drug Resistance. *Front Pharmacol*. 2021;12:648407.
8. Kikuchi M, Hara N, Hasegawa M, Miyashita A, Kuwano R, Ikeuchi T, Nakaya A. Enhancer variants associated with Alzheimer's disease affect gene expression via chromatin looping. *BMC Medical Genomics*. 2019;12(1):1-16.
9. Zhao L, Zhang B. Doxorubicin induces cardiotoxicity through upregulation of death receptors mediated apoptosis in cardiomyocytes. *Scientific Reports*. 2017;7(1):44735.
10. Christowitz C, Davis T, Isaacs A, Van Niekerk G, Hattingh S, Engelbrecht A-M. Mechanisms of doxorubicin-induced drug resistance and drug resistant tumour growth in a murine breast tumour model. *BMC Cancer*. 2019;19(1).
11. Kanwal U, Irfan Bukhari N, Ovais M, Abass N, Hussain K, Raza A. Advances in nano-delivery systems for doxorubicin: an updated insight. *Journal of drug targeting*. 2018;26(4):296-310.
12. Mi Y, Zhang J, Tan W, Miao Q, Li Q, Guo Z. Preparation of Doxorubicin-Loaded Carboxymethyl- β -Cyclodextrin/Chitosan Nanoparticles with Antioxidant, Antitumor Activities and pH-Sensitive Release. *Marine Drugs*. 2022;20(5):278.

13. Islam MM, Shahrizzaman M, Biswas S, Sakib MN, Rashid TU. Chitosan based bioactive materials in tissue engineering applications-A review. *Bioactive materials*. 2020;5(1):164-83.
14. Drozdova MG, Demina TS, Dregval OA, Gaidar AI, Andreeva ER, Zelenetskii AN, et al. Macroporous Hyaluronic Acid/Chitosan Polyelectrolyte Complex-Based Hydrogels Loaded with Hydroxyapatite Nanoparticles: Preparation, Characterization and In Vitro Evaluation. *Polysaccharides*. 2022;3(4):745-60.
15. Katuwavila NP, Perera ADLC, Samarakoon SR, Soysa P, Karunaratne V, Amaratunga GAJ, Karunaratne DN. Chitosan-Alginate Nanoparticle System Efficiently Delivers Doxorubicin to MCF-7 Cells. *Journal of Nanomaterials*. 2016;2016:1-12.
16. Cheung R, Ng T, Wong J, Chan W. Chitosan: An Update on Potential Biomedical and Pharmaceutical Applications. *Marine Drugs*. 2015;13(8):5156-86.
17. George M, Abraham TE. Polyionic hydrocolloids for the intestinal delivery of protein drugs: alginate and chitosan—a review. *Journal of controlled release*. 2006;114(1):1-14.
18. Weng W, Goel A, editors. *Curcumin and colorectal cancer: an update and current perspective on this natural medicine*. Seminars in cancer biology; 2022: Elsevier.
19. Xie H, Huang G, Zou J, Zhu Q, Liang Z, Huang X, et al. The Pharmacological Mechanism of Curcumin against Drug Resistance in Non-Small Cell Lung Cancer: Findings of Network Pharmacology and Bioinformatics Analysis. *Evidence-Based Complementary and Alternative Medicine*. 2022;2022.
20. Shaikh S, Shaikh J, Naba YS, Doke K, Ahmed K, Yusufi M. Curcumin: Reclaiming the lost ground against cancer resistance. *Cancer Drug Resistance*. 2021;4(2):298.
21. Sung H, Ferlay J, Siegel RL, Laversanne M, Soerjomataram I, Jemal A, Bray F. Global Cancer Statistics 2020: GLOBOCAN Estimates of Incidence and Mortality Worldwide for 36 Cancers in 185 Countries. *CA: A Cancer Journal for Clinicians*. 2021;71(3):209-49.
22. Contaldo F, Santarpia L, Cioffi I, Pasanisi F. Nutrition Transition and Cancer. *Nutrients*. 2020;12(3):795.
23. McCabe M, Perner Y, Magobo R, Mirza S, Penny C. Descriptive epidemiological study of South African colorectal cancer patients at a Johannesburg Hospital Academic institution. *JGH Open*. 2020;4(3):360-7.
24. De Renzi G, Gaballo G, Gazzaniga P, Nicolazzo C. Molecular Biomarkers according to Primary Tumor Location in Colorectal Cancer: Current Standard and New Insights. *Oncology*. 2021;99(3):135-43.

25. Migliore L, Migheli F, Spisni R, Coppedè F. Genetics, cytogenetics, and epigenetics of colorectal cancer. *Journal of Biomedicine and Biotechnology*. 2011;2011.
26. Simon K. Colorectal cancer development and advances in screening. *Clinical interventions in aging*. 2016;967-76.
27. Balchen V, Simon K. Colorectal cancer development and advances in screening. *Clinical Interventions in Aging*. 2016;Volume 11:967-76.
28. Nouraie M, Ashktorab H, Atefi N, Azam S, Tarjoman T, Lee E, et al. Can the rate and location of sessile serrated polyps be part of colorectal Cancer disparity in African Americans? *BMC Gastroenterology*. 2019;19(1).
29. Hossain MS, Karuniawati H, Jairoun AA, Urbi Z, Ooi DJ, John A, et al. Colorectal cancer: a review of carcinogenesis, global epidemiology, current challenges, risk factors, preventive and treatment strategies. *Cancers*. 2022;14(7):1732.
30. Sierra MS, Forman D. Burden of colorectal cancer in Central and South America. *Cancer Epidemiol*. 2016;44 Suppl 1:S74-S81.
31. Baranova A, Krasnoselskyi M, Starikov V, Kartashov S, Zhulkevych I, Vlasenko V, et al. Triple-negative breast cancer: current treatment strategies and factors of negative prognosis. *Journal of medicine and life*. 2022;15(2):153.
32. Rajakannu M, Magdeleinat P, Vibert E, Ciacio O, Pittau G, Innominato P, et al. Is cure possible after sequential resection of hepatic and pulmonary metastases from colorectal cancer? *Clinical Colorectal Cancer*. 2018;17(1):41-9.
33. Abraha I, Aristei C, Palumbo I, Lupattelli M, Trastulli S, Ciocchi R, et al. Preoperative radiotherapy and curative surgery for the management of localised rectal carcinoma. *Cochrane Database of Systematic Reviews*. 2018(10).
34. Nurgali K, Jagoe RT, Abalo R. Adverse effects of cancer chemotherapy: Anything new to improve tolerance and reduce sequelae? : *Frontiers Media SA*; 2018. p. 245.
35. Amjad MT, Chidharla A, Kasi A. *Cancer chemotherapy*. 2020.
36. Sun Y, Liu Y, Ma X, Hu H. The influence of cell cycle regulation on chemotherapy. *International Journal of Molecular Sciences*. 2021;22(13):6923.
37. Singhal V, Singh J, Lyall A, Saxena S, Bansal A. Is drug-induced toxicity a good predictor of response to neo-adjuvant chemotherapy in patients with breast cancer?-A prospective clinical study. *BMC cancer*. 2004;4:1-9.
38. Van Der Zanden SY, Qiao X, Neefjes J. New insights into the activities and toxicities of the old anticancer drug doxorubicin. *The FEBS Journal*. 2021;288(21):6095-111.

39. Bandyopadhyay D, Lopez G, Cantu S, Balboa S, Garcia A, Silva C, Valdes D. Key Enzymes in Cancer: Mechanism of Action and Inhibition With Anticancer Agents. 2018.
40. Mross K, Maessen P, Van Der Vijgh W, Gall H, Boven E, Pinedo H. Pharmacokinetics and metabolism of epidoxorubicin and doxorubicin in humans. *Journal of Clinical Oncology*. 1988;6(3):517-26.
41. Eikenberry S. A tumor cord model for doxorubicin delivery and dose optimization in solid tumors. *Theoretical Biology and Medical Modelling*. 2009;6:1-20.
42. W Edwardson D, Narendrula R, Chewchuk S, Mispel-Beyer K, PJ Mapletoft J, M Parissenti A. Role of drug metabolism in the cytotoxicity and clinical efficacy of anthracyclines. *Current drug metabolism*. 2015;16(6):412-26.
43. Wenningmann N, Knapp M, Ande A, Vaidya TR, Ait-Oudhia S. Insights into Doxorubicin-induced Cardiotoxicity: Molecular Mechanisms, Preventive Strategies, and Early Monitoring. *Molecular Pharmacology*. 2019;96(2):219-32.
44. Wang P, Yang HL, Yang YJ, Wang L, Lee SC. Overcome cancer cell drug resistance using natural products. *Evidence-Based Complementary and Alternative Medicine*. 2015;2015.
45. Catalano A, Iacopetta D, Ceramella J, Scumaci D, Giuzio F, Saturnino C, et al. Multidrug Resistance (MDR): A Widespread Phenomenon in Pharmacological Therapies. *Molecules*. 2022;27(3):616.
46. Li Y-J, Lei Y-H, Yao N, Wang C-R, Hu N, Ye W-C, et al. Autophagy and multidrug resistance in cancer. *Chinese Journal of Cancer*. 2017;36(1).
47. Housman G, Byler S, Heerboth S, Lapinska K, Longacre M, Snyder N, Sarkar S. Drug Resistance in Cancer: An Overview. *Cancers*. 2014;6(3):1769-92.
48. Moitra K. Overcoming Multidrug Resistance in Cancer Stem Cells. *BioMed Research International*. 2015;2015:1-8.
49. Hu T, Li Z, Gao C-Y, Cho CH. Mechanisms of drug resistance in colon cancer and its therapeutic strategies. *World Journal of Gastroenterology*. 2016;22(30):6876.
50. Lee G, Joung J-Y, Cho J-H, Son C-G, Lee N. Overcoming P-Glycoprotein-Mediated Multidrug Resistance in Colorectal Cancer: Potential Reversal Agents among Herbal Medicines. *Evidence-Based Complementary and Alternative Medicine*. 2018;2018:1-9.
51. Gao M, Miao L, Liu M, Li C, Yu C, Yan H, et al. miR-145 sensitizes breast cancer to doxorubicin by targeting multidrug resistance-associated protein-1. *Oncotarget*. 2016;7(37):59714-26.
52. Chakraborty A, Mahajan S, Jaiswal SK, Sharma VK. Genome sequencing of turmeric

provides evolutionary insights into its medicinal properties. *Communications Biology*. 2021;4(1).

53. Sivani BM, Azzeh M, Patnaik R, Pantea Stoian A, Rizzo M, Banerjee Y. Reconnoitering the Therapeutic Role of Curcumin in Disease Prevention and Treatment: Lessons Learnt and Future Directions. *Metabolites*. 2022;12(7):639.

54. Zhang X, Chen Q, Wang Y, Peng W, Cai H. Effects of curcumin on ion channels and transporters. *Frontiers in physiology*. 2014;5:94.

55. Sreenivasan S, Ravichandran S, Vetrivel U, Krishnakumar S. In vitro and In silico studies on inhibitory effects of curcumin on multi drug resistance associated protein (MRP1) in retinoblastoma cells. *Bioinformatics*. 2012;8(1):13.

56. Chearwae W, Shukla S, Limtrakul P, Ambudkar SV. Modulation of the function of the multidrug resistance-linked ATP-binding cassette transporter ABCG2 by the cancer chemopreventive agent curcumin. *Molecular cancer therapeutics*. 2006;5(8):1995-2006.

57. Wu C-P, Ohnuma S, V Ambudkar S. Discovering natural product modulators to overcome multidrug resistance in cancer chemotherapy. *Current pharmaceutical biotechnology*. 2011;12(4):609-20.

58. Joshi P, Vishwakarma RA, Bharate SB. Natural alkaloids as P-gp inhibitors for multidrug resistance reversal in cancer. *European journal of medicinal chemistry*. 2017;138:273-92.

59. Majidinia M, Mirza-Aghazadeh-Attari M, Rahimi M, Mihanfar A, Karimian A, Safa A, Yousefi B. Overcoming multidrug resistance in cancer: Recent progress in nanotechnology and new horizons. *IUBMB Life*. 2020;72(5):855-71.

60. Ayers D, Nasti A. Utilisation of Nanoparticle Technology in Cancer Chemoresistance. *Journal of Drug Delivery*. 2012;2012:1-12.

61. Kapse-Mistry S, Govender T, Srivastava R, Yergeri M. Nanodrug delivery in reversing multidrug resistance in cancer cells. *Frontiers in pharmacology*. 2014;5:159.

62. Blanco E, Shen H, Ferrari M. Principles of nanoparticle design for overcoming biological barriers to drug delivery. *Nature Biotechnology*. 2015;33(9):941-51.

63. Khan I, Saeed K, Khan I. Nanoparticles: Properties, applications and toxicities. *Arabian journal of chemistry*. 2019;12(7):908-31.

64. Parente JF, Sousa VI, Marques JF, Forte MA, Tavares CJ. Biodegradable Polymers for Microencapsulation Systems. *Advances in Polymer Technology*. 2022;2022:1-43.

65. Bhunchu S, Rojsitthisak P. Biopolymeric alginate-chitosan nanoparticles as drug

delivery carriers for cancer therapy. *Die Pharmazie-An International Journal of Pharmaceutical Sciences*. 2014;69(8):563-70.

66. Santos VP, Marques NS, Maia PC, Lima MABd, Franco LdO, Campos-Takaki GMd. Seafood waste as attractive source of chitin and chitosan production and their applications. *International journal of molecular sciences*. 2020;21(12):4290.

67. Younes I, Rinaudo M. Chitin and chitosan preparation from marine sources. Structure, properties and applications. *Marine drugs*. 2015;13(3):1133-74.

68. Nilsen-Nygaard J, Strand S, Vårum K, Draget K, Nordgård C. Chitosan: Gels and Interfacial Properties. *Polymers*. 2015;7(3):552-79.

69. Seyam S, Nordin NA, Alfatama M. Recent Progress of Chitosan and Chitosan Derivatives-Based Nanoparticles: Pharmaceutical Perspectives of Oral Insulin Delivery. *Pharmaceuticals*. 2020;13(10):307.

70. Abourehab MA, Rajendran RR, Singh A, Pramanik S, Shrivastav P, Ansari MJ, et al. Alginate as a Promising Biopolymer in Drug Delivery and Wound Healing: A Review of the State-of-the-Art. *International Journal of Molecular Sciences*. 2022;23(16):9035.

71. Zhang H, Cheng J, Ao Q. Preparation of Alginate-Based Biomaterials and Their Applications in Biomedicine. *Marine Drugs*. 2021;19(5):264.

72. Niculescu A-G, Grumezescu AM. Applications of chitosan-alginate-based nanoparticles—An up-to-date review. *Nanomaterials*. 2022;12(2):186.

73. Shalapy A, Zhao S, Zhang C, Li Y, Geng H, Ullah S, et al. Adsorption of Deoxynivalenol (DON) from Corn Steep Liquor (CSL) by the Microsphere Adsorbent SA/CMC Loaded with Calcium. *Toxins*. 2020;12(4):208.

74. Abasalizadeh F, Moghaddam SV, Alizadeh E, Akbari E, Kashani E, Fazljou SMB, et al. Alginate-based hydrogels as drug delivery vehicles in cancer treatment and their applications in wound dressing and 3D bioprinting. *Journal of biological engineering*. 2020;14:1-22.

75. Sarmento B, Ribeiro A, Veiga F, Ferreira D, Neufeld R. Insulin-loaded nanoparticles are prepared by alginate ionotropic pre-gelation followed by chitosan polyelectrolyte complexation. *Journal of nanoscience and nanotechnology*. 2007;7(8):2833-41.

76. Smitha B, Sridhar S, Khan A. Chitosan–sodium alginate polyion complexes as fuel cell membranes. *European Polymer Journal*. 2005;41(8):1859-66.

77. Sæther HV, Holme HK, Maurstad G, Smidsrød O, Stokke BT. Polyelectrolyte complex formation using alginate and chitosan. *Carbohydrate Polymers*. 2008;74(4):813-21.

78. Kulig D, Zimoch-Korzycka A, Jarmoluk A, Marycz K. Study on Alginate–Chitosan

Complex Formed with Different Polymers Ratio. *Polymers*. 2016;8(5):167.

79. Yoncheva K, Merino M, Shenol A, Daskalov NT, Petkov PS, Vayssilov GN, Garrido MJ. Optimization and in-vitro/in-vivo evaluation of doxorubicin-loaded chitosan-alginate nanoparticles using a melanoma mouse model. *International journal of pharmaceutics*. 2019;556:1-8.

80. Yoncheva K, Tzankov B, Yordanov Y, Spassova I, Kovacheva D, Frosini M, et al. Encapsulation of doxorubicin in chitosan-alginate nanoparticles improves its stability and cytotoxicity in resistant lymphoma L5178 MDR cells. *Journal of Drug Delivery Science and Technology*. 2020;59:101870.

81. Stetefeld J, McKenna SA, Patel TR. Dynamic light scattering: a practical guide and applications in biomedical sciences. *Biophysical reviews*. 2016;8:409-27.

82. Karell-Albo JA, Legón-Pérez CM, Madarro-Capó EJ, Rojas O, Sosa-Gómez G. Measuring independence between statistical randomness tests by mutual information. *Entropy*. 2020;22(7):741.

83. Sikkander AM, Yasmeen K. Characterization of Bacterial Culture on ZnO and Pb (NO₃)₂ Nanoparticles.

84. KALITA OCP, DOLEY P, Kalita A. 2. USES OF TRANSMISSION ELECTRON MICROSCOPE IN MICROSCOPY AND ITS ADVANTAGES AND DISADVANTAGES by OP CHOUDHARY, PC KALITA, PJ DOLEY AND A. KALITA. *Life Sciences Leaflets*. 2017;85:8 to 13-8 to

85. Ratner BD, Hoffman AS, Schoen FJ, Lemons JE. *Biomaterials science: an introduction to materials in medicine*: Elsevier; 2004.

86. Lin P-C, Lin S, Wang PC, Sridhar R. Techniques for physicochemical characterization of nanomaterials. *Biotechnology advances*. 2014;32(4):711-26.

87. Lewczuk B, Szyryńska N. Field-emission scanning electron microscope as a tool for large-area and large-volume ultrastructural studies. *Animals*. 2021;11(12):3390.

88. Johal MS, Johnson LE. *Understanding nanomaterials*: CRC Press; 2018.

89. Ghomrasni NB, Chivas-Joly C, Devuille L, Hochepeid J-F, Feltin N. Challenges in sample preparation for measuring nanoparticles size by scanning electron microscopy from suspensions, powder form and complex media. *Powder Technology*. 2020;359:226-37.

90. Tkachenko Y, Niedzielski P. FTIR as a Method for Qualitative Assessment of Solid Samples in Geochemical Research: A Review. *Molecules*. 2022;27(24):8846.

91. Othman N. IR Spectroscopy in Qualitative and Quantitative Analysis. *Infrared*

Spectroscopy-Perspectives and Applications: IntechOpen; 2022.

92. Zarina Z, Ruzaidi C, Sam S, Al Bakri AM, editors. Investigation on antioxidants compounds composition contains in *Leucaena Leucocephala* (Petai Belalang). IOP Conference Series: Materials Science and Engineering; 2019: IOP Publishing.
93. Jedrzejczak-Silicka M, Mijowska E. General cytotoxicity and its application in nanomaterial analysis. Cytotoxicity; IntechOpen: London, UK. 2018:177-205.
94. Mosmann T. Rapid colorimetric assay for cellular growth and survival: application to proliferation and cytotoxicity assays. *Journal of immunological methods*. 1983;65(1-2):55-63.
95. Leary M, Heerboth S, Lapinska K, Sarkar S. Sensitization of drug resistant cancer cells: a matter of combination therapy. *Cancers*. 2018;10(12):483.
96. Hiebl V, Schachner D, Ladurner A, Heiss EH, Stangl H, Dirsch VM. Caco-2 cells for measuring intestinal cholesterol transport-possibilities and limitations. *Biological Procedures Online*. 2020;22(1):1-18.
97. Pinto M. Enterocyte-like differentiation and polarization of the human colon carcinoma cell line Caco-2 cell culture. *Biol cell*. 1983;47:323-30.
98. Hauri H-P, Sterchi EE, Bienz D, Fransen J, Marxer A. Expression and intracellular transport of microvillus membrane hydrolases in human intestinal epithelial cells. *The Journal of cell biology*. 1985;101(3):838-51.
99. Kawahara I, Nishikawa S, Yamamoto A, Kono Y, Fujita T. The impact of breast cancer resistance protein (BCRP/ABCG2) on drug transport across Caco-2 cell monolayers. *Drug Metabolism and Disposition*. 2020;48(6):491-8.
100. Akhtar R, Chandel S, Sarotra P, Medhi B. Current status of pharmacological treatment of colorectal cancer. *World journal of gastrointestinal oncology*. 2014;6(6):177.
101. Sethy C, Kundu CN. 5-Fluorouracil (5-FU) resistance and the new strategy to enhance the sensitivity against cancer: Implication of DNA repair inhibition. *Biomedicine & Pharmacotherapy*. 2021;137:111285.
102. Zhang J, Huang H, Xue L, Zhong L, Ge W, Song X, et al. On-demand drug release nanoplatfrom based on fluorinated aza-BODIPY for imaging-guided chemo-phototherapy. *Biomaterials*. 2020;256:120211.
103. Cukierman E, Khan DR. The benefits and challenges associated with the use of drug delivery systems in cancer therapy. *Biochemical pharmacology*. 2010;80(5):762-70.
104. Wong KH, Lu A, Chen X, Yang Z. Natural ingredient-based polymeric nanoparticles for cancer treatment. *Molecules*. 2020;25(16):3620.

105. Yang F, Teves SS, Kemp CJ, Henikoff S. Doxorubicin, DNA torsion, and chromatin dynamics. *Biochimica et Biophysica Acta (BBA)-Reviews on Cancer*. 2014;1845(1):84-9.
106. Guo F, Yu N, Jiao Y, Hong W, Zhou K, Ji X, et al. Star polyester-based folate acid-targeting nanoparticles for doxorubicin and curcumin co-delivery to combat multidrug-resistant breast cancer. *Drug Delivery*. 2021;28(1):1709-21.
107. Farghadani R, Naidu R. Curcumin as an enhancer of therapeutic efficiency of chemotherapy drugs in breast cancer. *International Journal of Molecular Sciences*. 2022;23(4):2144.
108. Keyvani-Ghamsari S, Khorsandi K, Gul A. Curcumin effect on cancer cells' multidrug resistance: an update. *Phytotherapy research*. 2020;34(10):2534-56.
109. Willenbacher E, Khan SZ, Mujica SCA, Trapani D, Hussain S, Wolf D, et al. Curcumin: new insights into an ancient ingredient against cancer. *International journal of molecular sciences*. 2019;20(8):1808.
110. Li S, Wang X-t, Zhang X-b, Yang R-j, Zhang H-z, Zhu L-z, Hou X-p. Studies on alginate–chitosan microcapsules and renal arterial embolization in rabbits. *Journal of controlled release*. 2002;84(3):87-98.
111. Kumar S, Chauhan N, Gopal M, Kumar R, Dilbaghi N. Development and evaluation of alginate–chitosan nanocapsules for controlled release of acetamiprid. *International journal of biological macromolecules*. 2015;81:631-7.
112. Douglas KL, Piccirillo CA, Tabrizian M. Effects of alginate inclusion on the vector properties of chitosan-based nanoparticles. *Journal of controlled release*. 2006;115(3):354-61.
113. Loquercio A, Castell-Perez E, Gomes C, Moreira RG. Preparation of Chitosan-Alginate Nanoparticles for *Trans*-cinnamaldehyde Entrapment. *Journal of Food Science*. 2015;80(10):N2305-N15.
114. Kaur I, Ellis L-J, Romer I, Tantra R, Carriere M, Allard S, et al. Dispersion of nanomaterials in aqueous media: Towards protocol optimization. *Journal of visualized experiments: JoVE*. 2017(130).
115. Correia M, Uusimäki T, Philippe A, Loeschner K. Challenges in determining the size distribution of nanoparticles in consumer products by asymmetric flow field-flow fractionation coupled to inductively coupled plasma-mass spectrometry: the example of Al₂O₃, TiO₂, and SiO₂ nanoparticles in toothpaste. *Separations*. 2018;5(4):56.
116. Li N, Li X, Cheng P, Yang P, Shi P, Kong L, Liu H. Preparation of Curcumin Solid Lipid Nanoparticles Loaded with Flower-Shaped Lactose for Lung Inhalation and Preliminary

Evaluation of Cytotoxicity In Vitro. Evidence-Based Complementary and Alternative Medicine. 2021;2021:1-15.

117. Baskin TI, Orr TJ, Jercinovic M, Yoshida M. Sample preparation for scanning electron microscopy: the surprising case of freeze drying from tertiary butanol. *Microscopy Today*. 2014;22(3):36-9.

118. Parveen S, Sahoo SK. Evaluation of cytotoxicity and mechanism of apoptosis of doxorubicin using folate-decorated chitosan nanoparticles for targeted delivery to retinoblastoma. *Cancer Nanotechnology*. 2010;1(1-6):47-62.

119. Patil J, Kamalapur M, Marapur S, Kadam D. Ionotropic gelation and polyelectrolyte complexation: the novel techniques to design hydrogel particulate sustained, modulated drug delivery system: a review. *Digest Journal of Nanomaterials and Biostructures*. 2010;5(1):241-8.

120. Gupta VK, Karar P. Optimization of process variables for the preparation of chitosan-alginate nanoparticles. *Int J pharm pharm sci*. 2011;3(2):78-80.

121. Mokhtari S, Jafari SM, Assadpour E. Development of a nutraceutical nano-delivery system through emulsification/internal gelation of alginate. *Food chemistry*. 2017;229:286-95.

122. Barth HG. *Modern methods of particle size analysis*: John Wiley & Sons; 1984.

123. Jayakumar R, Prabakaran M, Kumar PS, Nair S, Tamura H. Biomaterials based on chitin and chitosan in wound dressing applications. *Biotechnology advances*. 2011;29(3):322-37.

124. Friedman AJ, Phan J, Schairer DO, Champer J, Qin M, Pirouz A, et al. Antimicrobial and anti-inflammatory activity of chitosan–alginate nanoparticles: a targeted therapy for cutaneous pathogens. *Journal of investigative Dermatology*. 2013;133(5):1231-9.

125. Dubey R, Bajpai J, Bajpai A. Chitosan-alginate nanoparticles (CANPs) as potential nanosorbent for removal of Hg (II) ions. *Environmental Nanotechnology, Monitoring & Management*. 2016;6:32-44.

126. Azevedo MA, Bourbon AI, Vicente AA, Cerqueira MA. Alginate/chitosan nanoparticles for encapsulation and controlled release of vitamin B2. *International Journal of Biological Macromolecules*. 2014;71:141-6.

127. Rosyada A, Sunarharum W, Waziroh E, editors. *Characterization of chitosan nanoparticles as an edible coating material*. IOP Conference Series: Earth and Environmental Science; 2019: IOP Publishing.

128. Masarudin MJ, Cutts SM, Evison BJ, Phillips DR, Pigram PJ. Factors determining the

- stability, size distribution, and cellular accumulation of small, monodisperse chitosan nanoparticles as candidate vectors for anticancer drug delivery: application to the passive encapsulation of [14C]-doxorubicin. *Nanotechnology, science and applications*. 2015;67-80.
129. Ardani H, Imawan C, Handayani W, Djuhana D, Harmoko A, Fauzia V, editors. Enhancement of the stability of silver nanoparticles synthesized using aqueous extract of *Diospyros discolor* Willd. leaves using polyvinyl alcohol. *IOP Conference Series: Materials Science and Engineering*; 2017: IOP Publishing.
130. Taghe S, Mirzaeei S. Preparation and characterization of novel, mucoadhesive ofloxacin nanoparticles for ocular drug delivery. *Brazilian Journal of Pharmaceutical Sciences*. 2019;55.
131. Sorasitthiyankarn FN, Bhuket PRN, Muangnoi C, Rojsitthisak P, Rojsitthisak P. Chitosan/alginate nanoparticles as a promising carrier of novel curcumin diethyl diglutarate. *International journal of biological macromolecules*. 2019;131:1125-36.
132. Krausz AE, Adler BL, Makdisi J, Schairer D, Rosen J, Landriscina A, et al. Nanoparticle-encapsulated doxorubicin demonstrates superior tumor cell kill in triple negative breast cancer subtypes intrinsically resistant to doxorubicin. *Precision nanomedicine*. 2018;1(3):173.
133. Sun D, Zhou S, Gao W. What went wrong with anticancer nanomedicine design and how to make it right. *ACS nano*. 2020;14(10):12281-90.
134. Motwani SK, Chopra S, Talegaonkar S, Kohli K, Ahmad FJ, Khar RK. Chitosan–sodium alginate nanoparticles as submicroscopic reservoirs for ocular delivery: Formulation, optimisation and in vitro characterisation. *European Journal of Pharmaceutics and Biopharmaceutics*. 2008;68(3):513-25.
135. Chernyshev VS, Rachamadugu R, Tseng YH, Belnap DM, Jia Y, Branch KJ, et al. Size and shape characterization of hydrated and desiccated exosomes. *Analytical and Bioanalytical Chemistry*. 2015;407(12):3285-301.
136. Zheng T, Bott S, Huo Q. Techniques for Accurate Sizing of Gold Nanoparticles Using Dynamic Light Scattering with Particular Application to Chemical and Biological Sensing Based on Aggregate Formation. *ACS Applied Materials & Interfaces*. 2016;8(33):21585-94.
137. Suopajärvi T. Functionalized nanocelluloses in wastewater treatment applications. *Acta Universitatis Ouluensis C*. 2015;526.
138. Villegas-Peralta Y, López-Cervantes J, Madera Santana TJ, Sánchez-Duarte RG, Sánchez-Machado DI, Martínez-Macías MdR, Correa-Murrieta MA. Impact of the molecular

weight on the size of chitosan nanoparticles: Characterization and its solid-state application. *Polymer Bulletin*. 2021;78:813-32.

139. Rajendran A, Basu SK. Alginate-chitosan particulate system for sustained release of nimodipine. *Tropical journal of pharmaceutical research*. 2009;8(5).

140. Chen G-L, Cai H-Y, Chen J-P, Li R, Zhong S-Y, Jia X-J, et al. Chitosan/Alginate Nanoparticles for the Enhanced Oral Antithrombotic Activity of Clam Heparinoid from the Clam *Coelomactra antiquata*. *Marine Drugs*. 2022;20(2):136.

141. Nandiyanto ABD, Oktiani R, Ragadhita R. How to read and interpret FTIR spectroscopy of organic material. *Indonesian Journal of Science and Technology*. 2019;4(1):97-118.

142. Bahuguna A, Khan I, Bajpai VK, Kang SC. MTT assay to evaluate the cytotoxic potential of a drug. *||| Bangladesh Journal of Pharmacology*. 2017;12(2):115-8.

143. Kamiloglu S, Sari G, Ozdal T, Capanoglu E. Guidelines for cell viability assays. *Food Frontiers*. 2020;1(3):332-49.

144. Ghasemi M, Turnbull T, Sebastian S, Kempson I. The MTT Assay: Utility, Limitations, Pitfalls, and Interpretation in Bulk and Single-Cell Analysis. *International Journal of Molecular Sciences*. 2021;22(23):12827.

145. Hamed AR, Abdel-Azim NS, Shams KA, Hammouda FM. Targeting multidrug resistance in cancer by natural chemosensitizers. *Bulletin of the National Research Centre*. 2019;43(1):1-14.

146. Riahi-Chebba I, Souid S, Othman H, Haoues M, Karoui H, Morel A, et al. The Phenolic compound Kaempferol overcomes 5-fluorouracil resistance in human resistant LS174 colon cancer cells. *Scientific reports*. 2019;9(1):1-20.

147. Xue X, Liang X-J. Overcoming drug efflux-based multidrug resistance in cancer with nanotechnology. *Chinese journal of cancer*. 2012;31(2):100.

148. Wu W, Dnyanmote AV, Nigam SK. Remote communication through solute carriers and ATP binding cassette drug transporter pathways: an update on the remote sensing and signaling hypothesis. *Molecular Pharmacology*. 2011;79(5):795-805.

149. BOYRAZ MÜ, SHEKHANY B, SÜZERGÖZ F. Cellular Imaging Analysis of MTT Assay Based on Tetrazolium Reduction. *Harran Üniversitesi Tıp Fakültesi Dergisi*. 2021;18(1):95-9.

150. Espíndola MR, Varotti FdP, Aguiar ACC, Andrade SN, Rocha EMMd. In vitro assessment for cytotoxicity screening of new antimalarial candidates. *Brazilian Journal of Pharmaceutical Sciences*. 2022;58.

151. Riss TL, Moravec RA, Niles AL, Duellman S, Benink HA, Worzella TJ, Minor L. Cell

viability assays. Assay Guidance Manual [Internet]. 2016.

152. Dong L, Xu W-W, Li H, Bi K-H. In vitro and in vivo anticancer effects of marmesin in U937 human leukemia cells are mediated via mitochondrial-mediated apoptosis, cell cycle arrest, and inhibition of cancer cell migration Retraction in/10.3892/or. 2021.8065. *Oncology reports*. 2018;39(2):597-602.

153. He Y, Zhu Q, Chen M, Huang Q, Wang W, Li Q, et al. The changing 50% inhibitory concentration (IC50) of cisplatin: a pilot study on the artifacts of the MTT assay and the precise measurement of density-dependent chemoresistance in ovarian cancer. *Oncotarget*. 2016;7(43):70803.

154. Carvalho FS, Burgeiro A, Garcia R, Moreno AJ, Carvalho RA, Oliveira PJ. Doxorubicin-induced cardiotoxicity: from bioenergetic failure and cell death to cardiomyopathy. *Medicinal research reviews*. 2014;34(1):106-35.

155. Deepa K, Singha S, Panda T. Doxorubicin nanoconjugates. *Journal of nanoscience and nanotechnology*. 2014;14(1):892-904.

156. Rosch JG, Brown AL, DuRoss AN, DuRoss EL, Sahay G, Sun C. Nanoalginates via inverse-micelle synthesis: doxorubicin-encapsulation and breast cancer cytotoxicity. *Nanoscale Research Letters*. 2018;13:1-10.

157. Carrick S, Parker S, Thornton C, Gherzi D, Simes J, Wilcken N. Single agent versus combination chemotherapy for metastatic breast cancer. *Cochrane Database of Systematic Reviews*. 2009;2021(5).

158. Motevalli SM, Eltahan AS, Liu L, Magrini A, Rosato N, Guo W, et al. Co-encapsulation of curcumin and doxorubicin in albumin nanoparticles blocks the adaptive treatment tolerance of cancer cells. *Biophysics Reports*. 2019;5(1):19-30.

159. Guo W, Song Y, Song W, Liu Y, Liu Z, Zhang D, et al. Co-delivery of doxorubicin and curcumin with polypeptide nanocarrier for synergistic lymphoma therapy. *Scientific Reports*. 2020;10(1):1-16.

160. Zhang N, Gao M, Wang Z, Zhang J, Cui W, Li J, et al. Curcumin reverses doxorubicin resistance in colon cancer cells at the metabolic level. *Journal of Pharmaceutical and Biomedical Analysis*. 2021;201:114129.

161. Khameneh ZR, Mohammadian M, Rasouli MA, Moradi Z, Ahmadi Z, Khiyavi AA. Effects of curcumin in combination with doxorubicin in human colorectal cancer cell line. *Asian Pacific Journal of Cancer Biology*. 2018;3(4):89-92.